Interpretation of infrared and Raman spectra of amorphous carbon nitrides

A. C. Ferrari,[1,*] S. E. Rodil,[1,2] and J. Robertson[1]

[1]*Department of Engineering, University of Cambridge, Cambridge CB2 1PZ, United Kingdom*
[2]*Instituto de Investigaciones en Materiales, Universidad Autónoma de México, Coyoacan, D. F. 04510 Mexico*
(Received 12 June 2002; revised manuscript received 24 January 2003; published 9 April 2003)

A general framework for the interpretation of infrared and Raman spectra of amorphous carbon nitrides is presented. In the first part of this paper we examine the infrared spectra. The peaks around 1350 and 1550 cm^{-1} found in the infrared spectrum of amorphous carbon nitride or hydrogenated and hydrogen-free amorphous carbon are shown to originate from the large dynamic charge of the more delocalized π bonding which occurs in more sp^2 bonded networks. The IR absorption decreases strongly when the π bonding becomes localized, as in tetrahedral amorphous carbon. Isotopic substitution is used to assign the modes to C=C skeleton modes, even those modes around 1600 cm^{-1} which become strongly enhanced by the presence of hydrogen. The infrared spectrum of carbon nitride may resemble the Raman spectrum at some excitation energy, but the infrared activity does not primarily result from nitrogen breaking the symmetry. In the second part we examine the Raman spectra. A general model is presented for the interpretation of the Raman spectra of amorphous carbon nitrides measured at any excitation energy. The Raman spectra can be explained in terms of an amorphous carbon based model, without need of extra peaks due to CN, NN, or NH modes. We classify amorphous carbon nitride films in four classes, according to the corresponding N-free film: a-C:N, a-C:H:N, ta-C:H:N, and ta-C:N. We analyze a wide variety of samples for the four classes and present the Raman spectra as a function of N content, sp^3 content, and band gap. In all cases, a multiwavelength Raman study allows a direct correlation of the Raman parameters with the N content, which is not generally possible for single wavelength excitation. The G peak dispersion emerges as a most informative parameter for Raman analysis. UV Raman enhances the sp^1 CN peak, which is usually too faint to be seen in visible excitation. As for N-free samples, UV Raman also enhances the C-C sp^3 bonds vibrations, allowing the sp^3 content to be quantified.

I. INTRODUCTION

This paper is composed of three main parts. Section II provides a full classification of bonding in carbon nitrides. Sections III, IV, and V present a general model for the interpretation of the Infrared spectra of any carbon film, with or without hydrogen and nitrogen. Sections VI, VII, VIII, and IX give a general model for the interpretation of the Raman spectra of amorphous carbon nitrides measured at any excitation energy. The three parts are self-contained and can be consulted separately and proper intersection references are given.

The prediction of Liu and Cohen[1] of a C_3N_4 phase with a bulk modulus and hardness higher than diamond has led to considerable research on carbon nitrides. Despite these efforts, there has been no agreed success on the synthesis of crystalline β-C_3N_4.[2,3] Many of the experiments produced instead amorphous carbon nitrides (a-CN_x), which are of interest in their own right.[2,3] They show promising tribological properties.[4,5] Indeed amorphous carbon nitride is presently used as a protective coating for many hard disks and read heads.[5,6] It is therefore important to be able to determine the bonding in carbon nitrides, especially with nondestructive characterization techniques such as Raman and Infrared (IR) spectroscopy, photoemission, and near edge x-ray absorption fine structure spectroscopy (NEXAFS).

Photoemission is used to probe the nitrogen bonding configuration in carbon nitrides,[7–9] based on the core level shifts at different sites. However, the core level shift is quite small due to the relatively small polarity of the C-N bond and their precise assignment is still debated.[10] NEXAFS and electron energy loss spectroscopy (EELS) are used to try to distinguish between sp^2 and sp^3 bonding at both the C and N sites based on the local conduction band structure.[10–13] Raman and IR spectroscopy are widely used nondestructive probes of the bonding in carbon systems and in carbon nitrides in particular.

In order to derive the models for general understanding of the IR and Raman spectra in all carbon nitrides, we first classify carbon nitrides into four types (Sec. II): (a) the mainly sp^2 bonded a-C:N produced by sputtering, (b) the mainly sp^3 bonded ta-C:N produced by cathodic arc, pulsed laser deposition or mass selected ion beam deposition, (c) plasma deposited a-C:H:N with moderate sp^3 content, and (d) ta-C:H:N prepared by a high plasma density source, with a higher sp^3 content and lower hydrogen content.

In Sec. III, IV, V we consider the IR spectra. In hydrogenated amorphous carbon (a-C:H), Fourier transform IR (FTIR) has been used to determine the C-H bonding configuration.[14–17] In carbon nitrides, FTIR is used to study the bonding preference of hydrogen to C or N sites,[8] as well as the presence of sp^1 CN bonds at ~2100 cm^{-1}. This paper focuses on the skeleton or network modes of carbon nitride in the IR spectrum below 2000 cm^{-1}, which is said to show features resembling the Raman spectra by Kaufman, Metin, and Saperstein.[18] This has been an influential work on the IR spectroscopy of a-CN_x, because it asserted the following.

(1) The D and G peaks, usually observed in Raman spec-

tra, become IR active in amorphous carbon nitrides since the nitrogen incorporation breaks the symmetry of the sp^2 domains.

(2) This allows "doing Raman with IR."

However, recently some groups contested this analysis.[19–23] Here we will argue that the main conclusions of Kaufman *et al.*[18] are wrong and give an alternative interpretation. We will note that introducing nitrogen is not necessary to give IR activity in the 1000–2000 cm^{-1} region of a-C, and to give peaks resembling the D and G in the Raman spectra. The main reason for the intensity changes upon nitrogen introduction is not the activation of the D and G Raman modes in the IR, but is a purely electronic effect. The similarity between the Raman spectra acquired at 488 or 514 nm and the IR spectra of some carbon nitrides is generally accidental, and does not hold overall.

The wave number, intensity and shape of the D and G peaks in Raman spectroscopy vary with the laser excitation energy, because the excitation is resonant with an electronic transition.[24] This fact in itself is enough to show that a similarity between a visible Raman spectrum and IR spectrum is, *a priori*, purely accidental.

We will analyze the IR spectra of the various nitrogen-free amorphous carbons in the region below 2000 cm^{-1}. We will prove how nitrogen is not necessary to have IR activity in the 1000–2000 cm^{-1} region and propose a new explanation for this IR activity. We then show how these ideas also account for the effect of nitrogen introduction on the IR spectra. We also show how the IR spectra of carbon nitrides can be classified into four distinct spectral shapes.

In Sec. VI, VII, VIII, and IX this paper provides a thorough analysis of the Raman spectra of the various forms of carbon nitride films measured at various excitation wavelengths. The Raman spectra of carbon nitrides measured at any excitation energy have a similar form to those of N-free amorphous carbons. We present a general model for their interpretation, extending our previous model for N-free carbon films[24,25] to carbon nitrides. This previous model will be summarized in Sec. VI. In this model, we note that the Raman spectra depend fundamentally just on the configuration of sp^2 sites. An important factor is how the Raman spectra vary with photon excitation wavelength. The Raman matrix element is magnified when the excitation resonates with an optical transition. Raman scattering in carbons is always a resonant process, in which those configurations whose band gaps match the excitation energy are preferentially excited. The phonon frequencies of each configuration vary uniformly with their band gaps, so this causes the Raman modes to disperse with excitation energy. This makes dispersion a powerful way to derive the sp^2 site configuration. It is particularly useful in more complex systems such as amorphous carbon nitrides where many bonding configurations are possible, even for a given composition and sp^2 content. Indeed, a main result of this paper is that a combination of visible and UV Raman gives a wealth of information on carbon nitrides, not available from a study at single wavelength. This makes resonant Raman scattering particularly useful for carbon nitrides. This contrasts with most previous Raman studies on carbon nitrides, which only used visible
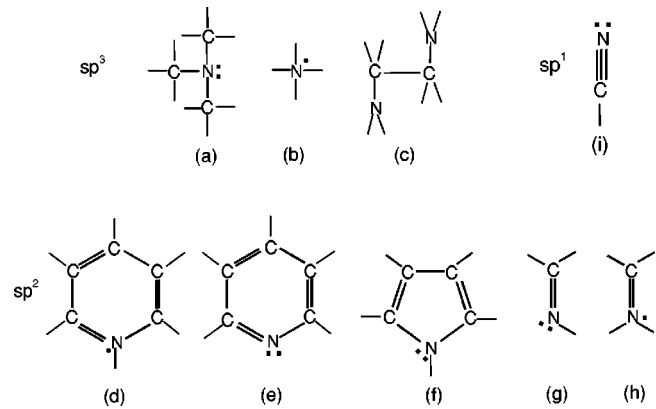

FIG. 1. The main bonding configurations of nitrogen in carbon nitrides, according to the hybridization of the surrounding carbons. Lines represent electron pair bonds. One dot means an unpaired electron. Two dots mean a nonbonding lone pair.

excitation.[4,19,23,26–30] Only a few workers used multi-wavelength excitation,[31–34] mainly performing UV Raman studies of ta-C:N.[31–33]

Previous studies focused on finding signatures for C-N bonds, N=N bonds, or N-H bonds in the Raman and IR spectra.[35–38] This paper adopts a different approach. The direct contribution of CN or NN or NH vibrations to the spectra will be neglected unless direct evidence of these is found.

II. CLASSIFICATION OF AMORPHOUS CARBON NITRIDES

It is convenient at this stage to summarize the main possible bonding configurations of nitrogen in carbon nitrides (Fig. 1).[39,40] In the simple trivalent configuration N_3^0, nitrogen forms three σ bonds with its remaining two valence electrons in a lone pair, Fig. 1(a). Nitrogen at a fourfold coordinated substitutional site N_4^+, uses four electrons in σ bonds with the remaining unpaired electron available for doping, Fig. 1(b). Another effect of N is to favor interlayer bonding. Substituting N for an sp^2 C breaks a π bond and leaves an unpaired electron of the remaining C available to form a σ bond to a similar atom on an adjacent layer, Fig. 1(c). The remaining configurations correspond to π bonding. N can substitute for carbon in a benzene ring to give a doping configuration, Fig. 1(d), or it can form a pyridinelike ring, Fig. 1(e). N can form a fivefold ring as in pyrrole, Fig. 1(f), where N uses three electrons in σ bonds and the other two are used to complete the aromatic sextet. These five-fold rings introduce warping in a graphitic layer. The other π bonded variants are olefinic nitrogen. In Fig. 1(g), N uses two electrons in σ bonds and one in a π bond, leaving a lone pair. In Fig. 1(h), N uses three electrons in σ bonds and 1 in a π bond and the fifth in an antibonding π^* state, available for doping. Finally, Fig. 1(i) in the nitrile group, a sp^1 N forms a triple bond and a lone pair. The doping configurations are included for completeness, but they are of low importance. In practice, starting from low N contents (~1%), N tends to induce π bonds and sp^2 clustering on carbon.[40]

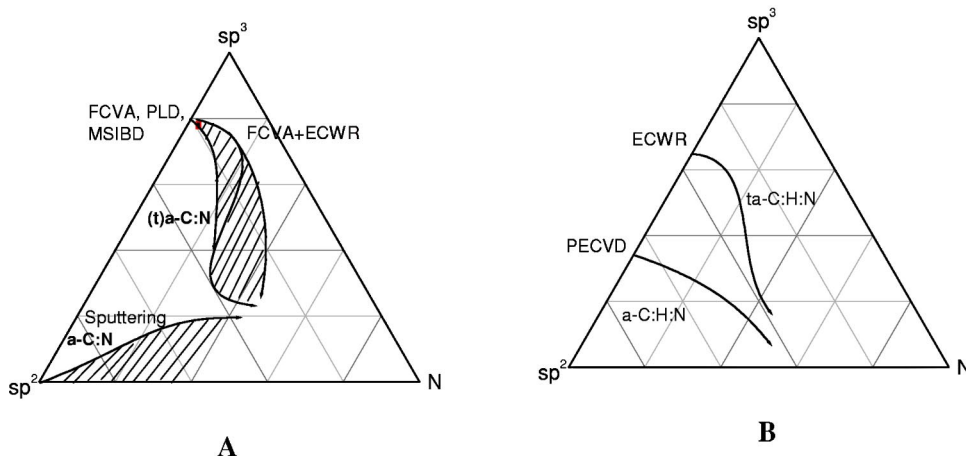It is possible to classify the bonding in carbon nitride

FIG. 2. Ternary phase diagrams of amorphous carbon nitride alloys, without hydrogen (a) or with hydrogen (b), showing sp^2 C, sp^3 C, and N.

films into four types, based on the bonding in the corresponding N-free film. The changes in the properties of the carbon nitride films as N content is increased should be compared with the properties of the corresponding N-free films. Thus, the variation of mechanical and electronic properties when N is added to a sp^2 bonded carbon film differs from when N is added to a high sp^3 film. This is true if H is present or not. There are four basic types of carbon nitride films, derived from sp^2 a-C, tetrahedral amorphous carbon (ta-C), a-C:H (from polymeric to diamondlike), and ta-C:H. Figure 2 shows the ternary phase diagrams which summarize the compositions of these four types of carbon nitrides with increasing N content.

(1) a-C:N. Amorphous carbon films with a high fraction of sp^2 bonded atoms are produced by dc, r.f. sputtering or magnetron sputtering and by low energy laser deposition. The introduction of N causes cross-linking between graphitic planes. An unusual aspect of these films is that a-C:N deposited above 200 °C can become nanostructured, with a strong crosslinking between graphitic planes, which gives an increase in mechanical hardness and large elastic recovery.[4,41–43]

(2) ta-C:N. This group includes films deposited by mass selected ion beam (MSIBD),[44] pulsed laser deposition (PLD),[45] or filtered cathodic vacuum arc (FCVA) (Refs. 29,46–49) either under N_2 atmospheres or by nitrogen assisted beams.[12] A low pressure deposition and high ionization degree ensures that the film growth is controlled by ions. The laser or arc is used to ablate a graphite target producing a highly ionized carbon beam under nitrogen background pressure. The nitrogen content increases as the N_2 background pressure is raised, but above a certain pressure a decrease in N content is usually observed.[50,51] Resistivity and optical gap decrease when compared to the pure ta-C films. Generally, the sp^3 content of ta-C remains high at 80–90 % up to about 10% N, and then the sp^3 content and density fall rapidly, as in Figs. 2(a) and 3.[29,45–49] This sharp decrease is due to the high deposition pressure.[12] A linear sp^3 vs N content relation was found when N assisted beams were used.[12] The sp^2 sites begin to cluster together at low N contents (1%), before the sp^3 to sp^2 transition, and this decreases the band gap, as shown in Fig. 4.[12,26,47,49,52–61]

(3) a-C:H:N. These films are usually grown by plasma enhanced chemical vapor deposition (PECVD).[8,26,27] a-C:H:N films have been deposited using a mixture of an hydrocarbon gas, such as methane, acetylene, benzene, and N_2 or NH_3. N incorporation is hindered if a high fraction of N_2 or a high substrate temperature is used. A maximum nitrogen content of ~20% is obtained for C_2H_2/N_2 mixtures;[62] the best conditions for nitrogen incorporation correspond to the lowest H content in the gas phase. The properties of a-C:H:N films are similar to the starting a-C:H film, due to the low N incorporation. In contrast to a-C:N, the hardness in a-C:H:N films decreases with N, due to the formation of more terminating groups, such as NH_2 and nitrile groups. Higher substrate temperatures and substrate bias decrease the overall N and H content, giving a more graphitelike material.

(4) ta-C:H:N. These films are prepared by an high density plasma source, such as the electron cyclotron wave resonance (ECWR),[23,62] electron cyclotron resonance (ECR),[63,64] or helicon sources.[65] Ta-C:H has much more C-C sp^3 bonding than a-C:H with similar sp^3 fraction. Introducing nitrogen into ta-C:H induces clustering of the sp^2 phase, without an appreciable sp^3 to sp^2 conversion, up to ~20% at N, with
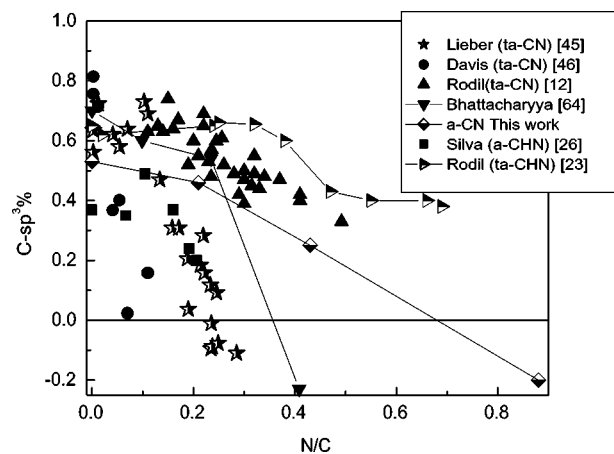

FIG. 3. Variation of C sp^3 bonding fraction with N content, for amorphous carbon nitrides prepared by different deposition techniques. Note that the ''negative'' C-sp^3 content values for some samples, effectively mean that we cannot neglect the C-sp^1 contribution in the analysis of the EELS K edge, see, e.g., Ref. 45.
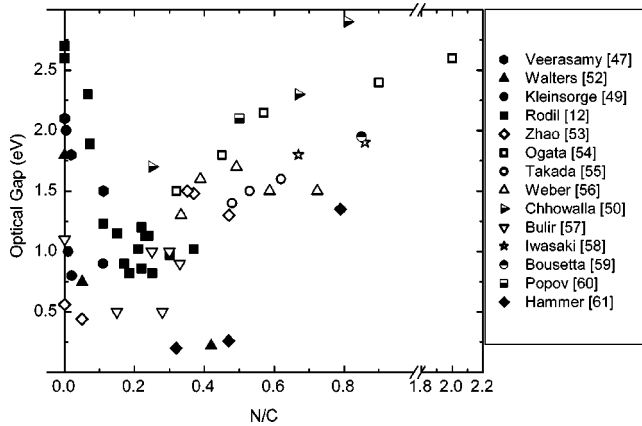
FIG. 4. Variation of optical gap with N/C ratio, for amorphous carbon nitrides prepared by different deposition techniques.
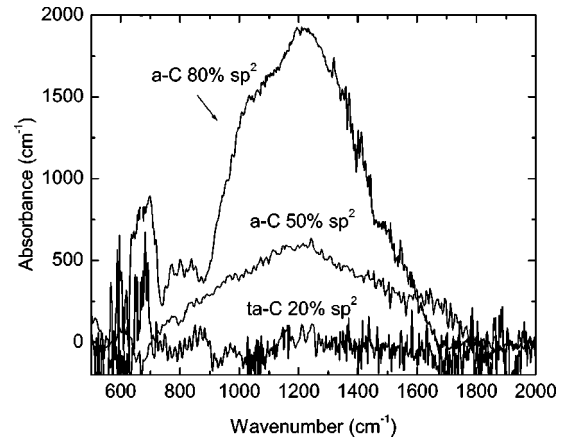

FIG. 5. Comparison of IR spectra of N-free amorphous carbon of increasing sp^2 content. The intensity has been normalized to take into account the different film thicknesses.

a corresponding increase in conductivity and decrease of optical gap. Higher N contents cause a transition to a lower sp^3 fraction and give softer films similar to polymeric a-C:H:N.[23,62]

Figures 2–4 summarize the changes in the main properties of these four classes of amorphous carbons as a function of N incorporation. In particular, Fig. 3 shows the variation of the sp^3 fraction with the N/C ratio. Note that, although a general decrease of sp^3 content with N is observed, the trends are different according to the deposition systems. This implies that the sp^3 fraction and the degree of clustering of the sp^2 phase can be different for films of the same N/C ratio.

The data used in Figs. 3 and 4 were derived with procedures consistent with the ones applied in this paper. In particular we selected papers were the sp^3 fraction was determined by EELS, the gap defined as the Tauc Gap from absorption and transmission measurements and the N content by RBS, EELS, and XPS measurements. The procedures used to derive the sp^3 content from EELS and the N content from RBS, EELS, and XPS for the samples discussed in this paper are described in detail in Refs. 12, 23, 62, and 66. The IR spectra in this paper are measured using a variety of FTIR spectrometers (BOMEM DA-3, ATI-Mattson RS1, Nicolet 205). An average of 200 scans per sample were taken while purging the spectrometer with N_2 or working in vacuum to reduce the signal from water vapor and CO_2.

III. IR SPECTRA OF NITROGEN-FREE AMORPHOUS CARBONS

Despite the efforts done to understand the vibrations of heteroatoms in the IR spectra of amorphous carbons,[14,15,67] there has been only limited work on understanding the skeletal vibrations in the sub 2000 cm^{-1} region. Consider the IR activity of a random covalent network. A homopolar crystal can be IR active if it has no center of symmetry, which requires three or more atoms in a unit cell. Thus, trigonal Se is active, while crystalline (c-)Si is inactive.[68] The random network of a-Si is IR active because the network no longer has a center of symmetry.[69] The loss of tetrahedral symmetry

means that the displacement of each Si atom creates an induced dipole on each bond, which no longer cancels out.

This situation also applies to the skeletal modes of amorphous carbon. In principle, the loss of symmetry means that all a-C networks should be IR active. There has been much less work on the skeletal modes of a-C below 2000 cm^{-1} than on the C-H modes. Knoll and Geiger[70] first reported the IR spectrum of sputtered a-C. Bonelli et $al.$[71] and Rodil et $al.$[23] reported the FTIR spectra of H-free (t)a-C samples, while Theye et $al.$[16,17] investigated this region for polymeric and diamondlike a-C:H.

Figure 5 compares the IR spectra of a sputtered a-C with about 80% sp^2 bonding, a ~50% sp^2 a-C, and a~20% sp^2 ta-C. The ta-C does not show any significant IR signal. However, for higher sp^2 content, the IR intensity increases and the most sp^2 bonded a-C sample has a clear IR spectrum, similar to that found by Knoll and Geiger.[70] The IR spectrum shows three main features at ~700, ~1250–1350 cm^{-1} and at 1550 cm^{-1}. Figure 5 allows us to propose a mechanism to explain the IR activity in amorphous carbons. It is clear that the sp^2 phase is mainly responsible, since the highest sp^3 sample has the lowest IR intensity. We can thus adopt a molecular approach, and ascribe IR activity to the sp^2 phase, which can be taken as a mixture of chains and rings of different size, order and relative proportion.

The IR spectra can be understood in terms of effective charges. The IR intensity is proportional to the sum of squares of the effective charges[72–74] for the vibrational modes Q_i

$$I \propto \sum_i \frac{(e_i^* e)^2}{m \omega_i^2}, \tag{1}$$

where e is the electronic charge, e^* is the effective charge for mode i, m is the reduced mass of mode i, and ω_i is its transverse frequency. The dipole moment is the product of the instantaneous ion charge q (static charge) and displacement

$$\mu = qr. \tag{2}$$

The effective charge $e*$ is the change in dipole moment for that mode

$$e* = \frac{\partial \mu}{\partial Q_i}. \tag{3}$$

Hence,

$$e* = \frac{\partial q}{\partial Q_i} r + q \frac{\partial r}{\partial Q_i}. \tag{4}$$

If we assume $q=0$ at the equilibrium position in a homopolar solid, the second term in Eq. (4) is zero. This is the case for H-and N-free samples. However, the first term can be nonzero. It is called the dynamic charge in solid state[72] or the charge flux in the chemical literature.[75,76] This term cancels by symmetry for c-Si, but it is nonzero for lower symmetries. $e*$ can be expressed in terms of the electron-phonon coupling between the ground (g) and excited (e) states as[75–78]

$$e* = \sum_e \mu^{ge} \frac{\langle e | \frac{\partial H}{\partial Q_i} | g \rangle}{E_e - E_g}. \tag{5}$$

In a-Si, the IR activity originates from the σ bonds. In ta-C, the σ bonds have a much wider band gap, so they are less polarizable, and their IR activity is much less. $e*$ and the IR absorption is much larger in sp^2 a-C than ta-C for two reasons. The π states have a smaller energy gap $E_e - E_g$ than the σ bonds, and secondly the conjugated π bonding of sp^2 sites means that there can be long-range charge flow over a number of bonds. Both these effects give a much larger dynamic charge for π states. This also implies that $e*$ increases with delocalization, since the gap becomes smaller for increasing delocalization and $\mu^{\pi\pi^*}$ increases with delocalization.[75–78]

Hence, the main reason for the increase in the IR activity with sp^2 content is the network of delocalized, conjugated π bonds. In contrast, the remaining sp^2 sites in ta-C are localized in isolated π bonds, which gives a much smaller IR activity. Thus the sp^2 delocalization and not the sp^2 content is the crucial parameter, and this is demonstrated by the very superlinear increase of IR intensity with sp^2 content in Fig. 5.

This analysis extends in straightforward fashion to the IR spectra of a-C:H and then a-C:N films. Figure 6 compares the IR spectra of polymeric a-C:H (3.2 eV gap, $H = 40$ at. %) and diamondlike a-C:H films (1.6 eV gap, $H = 35$ at. %).[16,17] Figure 7 shows the evolution of the spectra due to post-deposition annealing up to 600 °C.[16,17]

The IR spectrum in the 1000–2000 cm^{-1} range has been examined in detail by Theye *et al.*[16,17] This region contains both C-C skeleton modes, sp^3 CH$_{2,3}$ bending modes at ~1375 cm^{-1} and 1460 cm^{-1}, and the 1705 cm^{-1} C=O mode, due to oxygen contamination in polymeric samples.[16,17] Here we do not focus on these modes, which have been studied extensively,[14,15] but on the remaining part of the spectra. Following Theye,[16,17] the contribution of CH$_x$
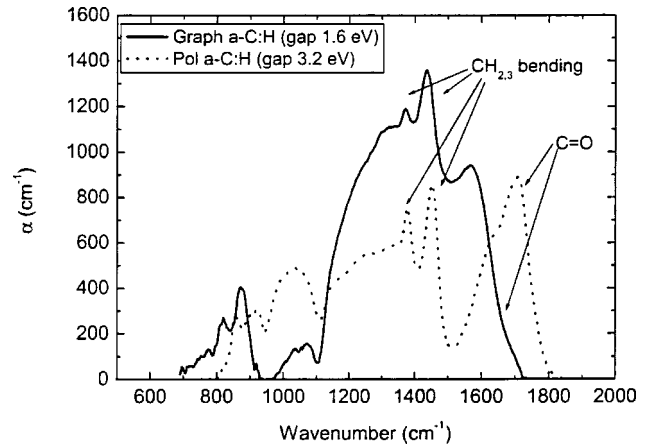

FIG. 6. Comparison of IR spectra of graphitic and polymeric a-C:H films, adapted from Refs. 16 and 17.

bending modes is removed by using H-D substitution to reveal the C-C skeletal modes, as in Figs. 8(a), and 8(b). This shows that the skeletal region consists of two broad bands at 1300–1400 and 1550–1580 cm^{-1}. The two bands are similar to those of H-free samples in Fig. 5, but with different intensities and positions. The main difference is the presence of a sharper peak at 1550 cm^{-1} and a clear dip between this peak and the 1300–1400 cm^{-1} band. It is tempting to ascribe this difference to C-H bonding. However, these peaks do not shift on deuterium substitution, so it is all due to C-C vibrations, and thus to the different C-C bond configuration in hydrogenated films.

Figure 7 shows that post-deposition annealing to 600 °C removes hydrogen, increases the intensity of the IR bands and the relative intensity of the ~1350 cm^{-1} band, removing the dip between this band and the higher frequency one. The spectra become more similar to the H-free ones of Fig. 5, even though the two main bands are shifted upwards and are sharper.

The effective charge model explains simply the spectra of Figs. 6–8. The polymeric a-C:H samples have a larger gap and more π localization than the diamondlike films, and this explains the lower IR intensity in Fig. 6. Annealing increases
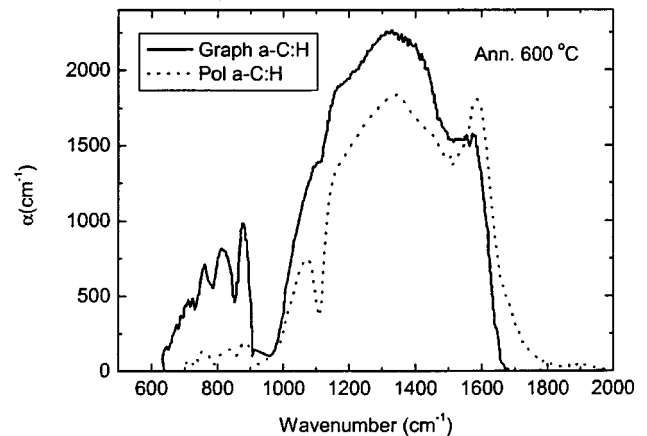

FIG. 7. Comparison of IR spectra IR spectra of annealed graphitic and polymeric a-C:H, adapted from Refs. 16 and 17.
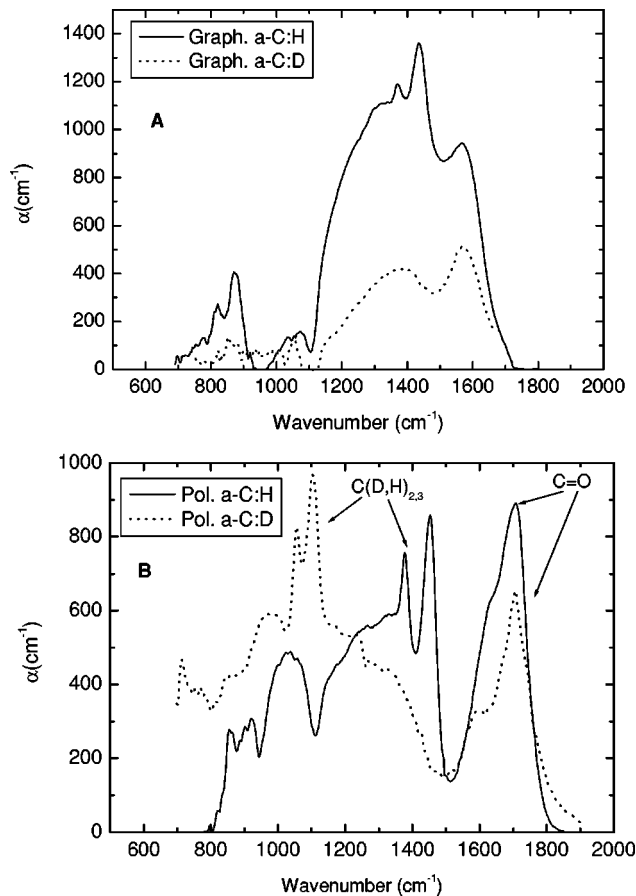
FIG. 8. Comparison of IR spectra of (a) graphitic a-C:H and a-C:D and (b) polymeric a-C:H and a-C:D, adapted from Refs. 16 and 17. The difference in intensity between the deuterated and hydrogenated samples can be ascribed to the slight difference in the band gap of these samples (Refs. 16, 17), according to Eq. (5).

FIG. 9. Comparison of IR spectrum of the four classes of carbon nitrides, (a) ta-C:N, 23 % at. N (b) ta-C:H:N, 28.7 at. % N, 26 % at. H, (c) a-C:H:N, 20% at. N, 35 % at. H (estimated values) (d) a-C:N, 31% N.

the sp^2 content and the π delocalization, thus giving a higher $e*$ and higher IR intensities, as observed in Fig. 7. Indeed, the spectrum shape and intensity of annealed a-C:H samples closely resemble one another in Fig. 7. Note how the activation of the D and G peak by symmetry breaking proposed by Kaufman et al.[18] would give a decrease of IR intensity with annealing, as annealing orders the samples and eventually increases the symmetries. This model therefore gives the opposite trend to that shown in Figs. 5–7.

IV. IR SPECTRA OF AMORPHOUS CARBON NITRIDES

The IR spectra of carbon nitrides resemble those of N-free amorphous carbons. This is because the C-N modes lie in a similar wave number range as the C-C modes, 1500–1600 cm^{-1} for sp^2 chain species, and 1300–1600 cm^{-1} for ring species.[67,79] Secondly, nitrogen encourages more sp^2 bonding and large cluster sizes, so the vibrational modes are delocalised and not confined to very specific configurations.

The effective charge arguments can be extended to carbon nitrides. Most IR spectra of carbon nitrides can be summarized in terms of four typical shapes, one for each of the four classes of a-C:(H):N described in Sec. II. The four classes
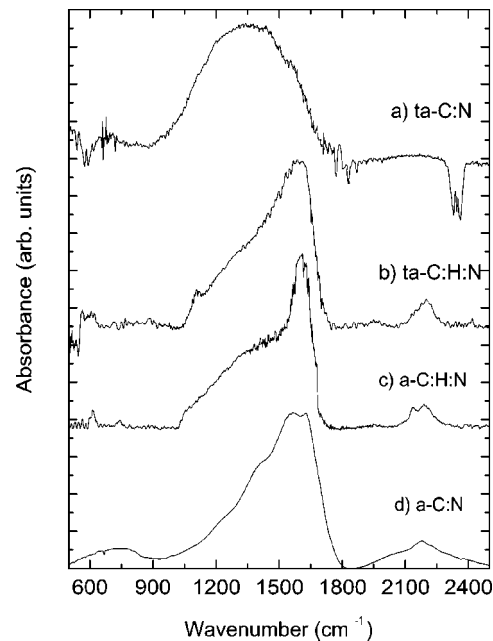
of IR spectra are shown in Fig. 9. The IR spectra of diamondlike a-C:H:N are very similar to those of ta-C:H:N, so we only consider a-C:H:N films with a high hydrogen content as a different case to ta-C:H:N. Note that the IR spectrum of the $(t)a$-C:N films in Fig. 9(a) is typical of the spectrum generally found for hard H-free films, such as classes 1 and 2 of Sec. II. The spectrum of Fig. 9(d) represents a peculiar group of carbon nitride samples which, independent of the deposition process, have an IR spectrum in the 3000–3300 cm^{-1} region dominated by H-related bands, even though hydrogen was not necessarily present during the deposition. These are low density, high porosity a-C:N and water is mainly incorporated through the formation of hydrogen bonds.[2] The IR spectra of these films can thus be assimilated to a-C:H:N rather that a-C:N. Indeed, we can reduce the spectra to only two main types, shown in Figs. 9(a) and 9(b), the H-free and hydrogenated carbon nitrides.

Comparing Fig. 9 and Figs. 5–8, there is a remarkable similarity between the IR spectra of N-free and N-containing films. In particular, the spectra of H-free films show only a single broad band with two modulations at ~1300 and ~1550 cm^{-1}, with slightly different intensity ratios. In contrast, films with hydrogen [such as polymeric a-C:H and $(t)a$-C:H:N grown from CH$_4$] show an increasingly well-defined peak at 1550–1600 cm^{-1}. We noted in Sec. III that all the features in the 1000–2000 cm^{-1} region in a-C:(H) (except the CH$_x$ bending, not seen in Fig. 9 anyway) are due to skeletal C=C vibrations. This argument suggests that all the features in Fig. 9 are due to C=C modes or mixed C=N modes, and *not* due to specific C-H, C-N, N-H, and N-N vibrations, as is sometimes claimed.[2,22]

This argument is supported by the effect of H-D and ^{14}N-^{15}N substitution on the IR spectra. We deposited
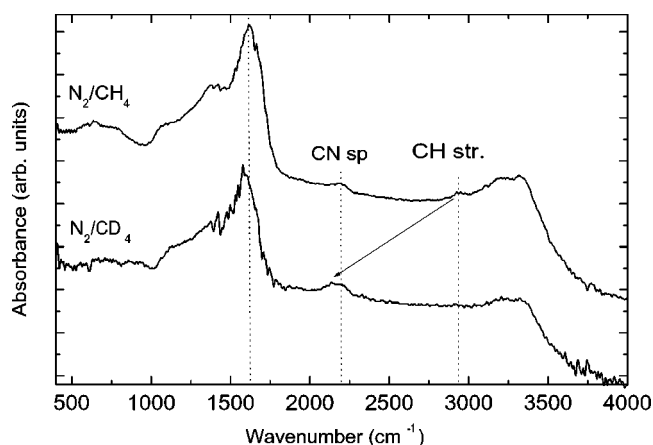
FIG. 10. Comparison of the IR spectra of a-C:H:N and deuterated a-C:D:N, showing the strong peak at 1600 cm^{-1} is not shifted by deuteration, as it would be expected if it was due to N-H, N-D bending.

ta-C:H:N films from N_2/CH$_4$ and N_2/CD$_4$ mixtures with an ECWR. This produced films with a high H content and a very sharp and intense peak at ~1580–1600 cm^{-1} (Fig. 10), almost twice as high as the broad band at 1300 cm^{-1}, and more intense even than in the previous isotopic substitution experiments of Victoria et $al.$[19] The 1590 cm^{-1} peak intensity seems to correlate with the appearance of modes at ~3300 cm^{-1} sometimes attributed to N-H stretching and with the higher H content.[62] It is thus tempting to attribute the peak to N-H bending, as often done, in parallel with the attribution of the ~3300 cm^{-1} modes to N-H stretching.[2] However, H-D substitution shows that this is wrong. Figure 10 shows that there is not the significant down shift required for deuterium substitution on a C-H or N-H mode. Hence, even if the sharp 1600 cm^{-1} peak is typical of a-C:H:N with an high H content, it is not due to a N-H mode, in the same way as the corresponding peak in polymeric a-C:H is not due to C-H bending. A similar conclusion was reached by Victoria et $al.$[19] for a-C:D:N samples with a less intense ~1580 cm^{-1} peak.

Victoria et $al.$[19] and Kaufman et $al.$[18] also studied ^{15}N-^{14}N substitution in a-C:N and a-C:H:N films. Although the mass difference is small, a measurable shift of wave numbers is still expected if specific N-related modes were involved. However again, few differences were found, and these could be attributed to little structural discrepancies in films grown in distinct runs. This suggests that N-N and C-N vibrations do not contribute to the spectra of Fig. 9.

Summarizing, isotope substitution shows that the IR spectra of Fig. 9 are due to skeletal C=C vibrations. Even if C-N bonds do create dipoles, the actual C-N vibrations associated with these dipoles do not contribute significantly to the IR spectra. On the other hand, it is generally found that nitrogen increases the intensity of these IR bands, at least up to N ~20%.[18] How does this happen if N does not directly contribute to these vibrations?

One effect of N is to introduce polar bonding and a static effective charge. However, the C-N bond is not very polar.[1] The main effect of nitrogen is thus to increase the static

charge on the carbon atoms to which N is bonded and, due to the presence of the π system, the polarization of the sp^2 skeleton and thus increase the dynamic effective charge $e*$. This can be understood if one considers that N, even if not directly contributing an extra electron to the π system, polarizes all the sp^2 bonds of the conjugated system to which is only a terminal atom. Thus it increases the bond dipole moment of each C-C bond, resulting in an effect which is larger for longer conjugation. This also explains the highly superlinear intensity increase with N introduction sometimes observed.[21] The effect of nitrogen is to break the electronic symmetry of the π system, whilst the effect of breaking the structural symmetry is per se negligible. Furthermore, N usually increases the sp^2 fraction and the clustering of the sp^2 phase, Figs. 3 and 4, and this also increases the IR intensity, as discussed in the previous section.

Fanchini et $al.$[21] use a related idea. They assign the shift of the G peak between the Raman and IR spectra of a given film to a LO-TO (longitudinal-optic–transverse-optic) splitting of a E mode, as in the Lyddane-Sachs-Teller (LST) relationship.[80] This is used to extract values for the ionic polarizability I and hence the effective charge $e*$ using Eq. (1). They estimate $e*{\sim}0.6e$ for a-C:H:N samples with ~10% N and ~15% H and ~0.7 eV gap. We note that this approach only works when the Raman spectra show little dispersion with excitation energy, as in the case considered in Ref. 21.

The integrated IR activity in the 1000–1800 cm^{-1} region can be used as an indication of N content. Figures 11(a)–11(c) show the variation of the integrated IR activity in the 1000–1800 cm^{-1} region in $(t)a$-C:N and $(t)a$-C:H:N samples as a function of N, sp^2 content, and gap. A clear correlation is seen with the N content, optical gap, and sp^2 content. This demonstrates that the integrated IR intensity is a useful parameter to characterize N-containing samples, even though it has been so far rarely considered. The precise trends may vary with the sample or deposition system, but the variations shown in Fig. 11 are enough to show the effect, the aim of this paper being the explanation of the overall IR intensity. Further studies are needed in order to account for the precise spectral shape and variation in peak positions for each of the classes shown in Fig. 9.

The effect of nitrogen in amorphous carbons is analogous to doping or photoexcitation in conjugated polymers such as polyenes and polyaromatic polymers.[75,81–83] It is known that doping induces very intense IR bands. This was once ascribed to mysterious Raman active modes. It was then shown[75,81–83] that the new modes arise from the breakdown of the electrical symmetry by the removal or injection of charges. The intensity of the IR modes is due to the very large charge fluxes and a longer conjugation length. The modes with high IR intensity tend to have the highest electron phonon coupling. The vibrations giving rise the maximum electron-phonon coupling are also the ones responsible for the highest Raman intensity modes in the undoped conjugated materials.[75,81–83] Only in the case of push-pull molecules, i.e., conjugated molecules terminated by a donor (D) and acceptor (A) groups forming a D-π-A system, the intramolecular charge transfer creates a strong link between IR
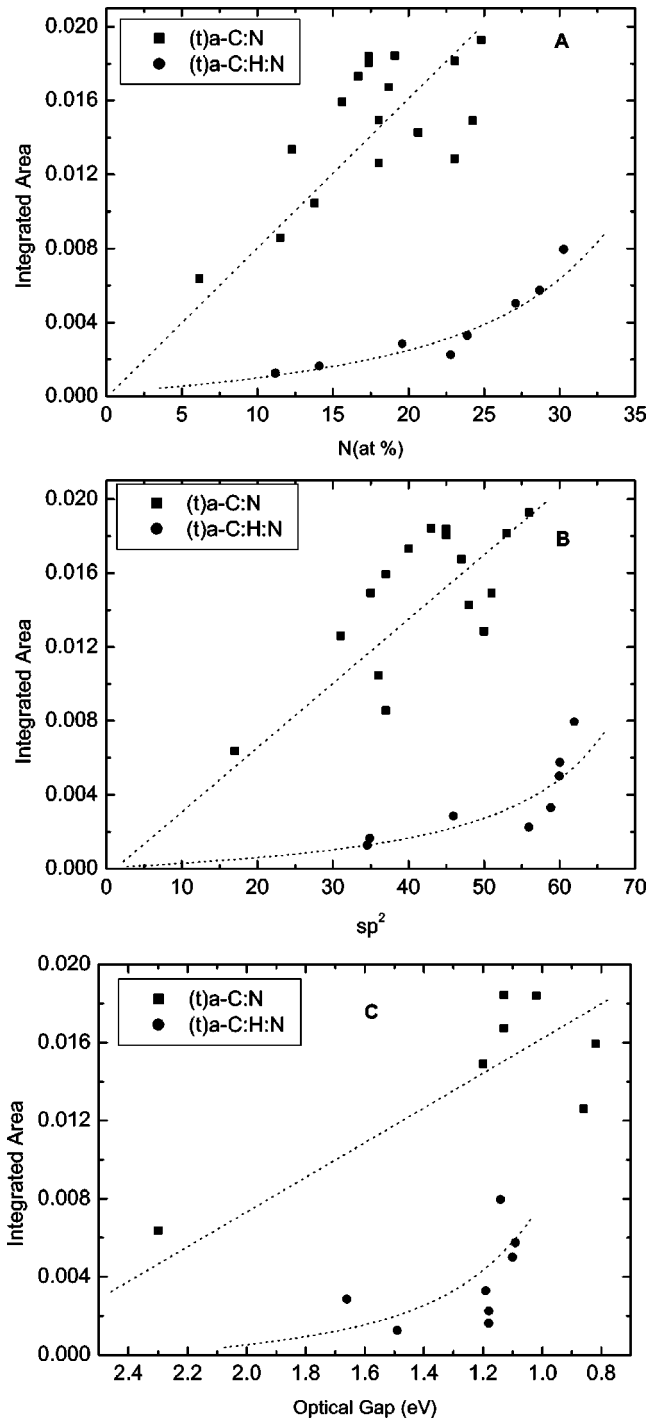
FIG. 11. Integrated IR absorbance, normalized to take into account the different film thicknesses, vs nitrogen content (a), sp^2 content (b), and optical gap (c) for a series of $(t)a$-C:N and $(t)a$-C:H:N. The lines are guides to the eye.
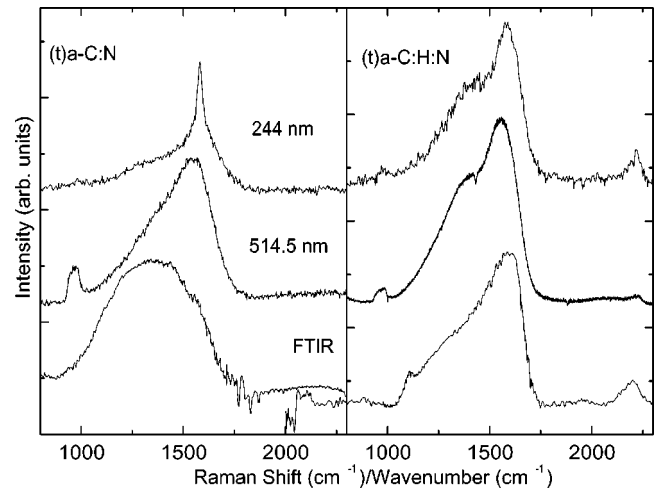

FIG. 12. Comparison of the IR spectra and the 514.5 and 244 nm Raman spectra for films representing the two main classes of amorphous carbon nitrides of Figs. 9(a) and 9(b).

and Raman active modes. In this case, the most prominent features in the Raman spectrum are also strongly active in the IR.[83]

V. CAN WE COMPARE IR AND RAMAN SPECTRA IN AMORPHOUS CARBON NITRIDES?

The following sections discuss the resonant Raman spectra of carbon nitrides. The apparent similarity between IR and visible Raman spectra still leads some to consider their equivalence, as for Ref. 18. However, Raman scattering is always a resonant process, so that the spectral shapes change with varying excitation energy. This in itself is enough to show that a similarity between the IR and Raman spectra taken at visible excitation is *a priori* purely accidental. Figure 12 compares the IR spectra and the 514 and 244 nm Raman spectra for the two main classes of carbon nitrides of Figs. 9(a) and 9(b). Whenever a fit in terms of the D and G peaks of the visible Raman and IR spectral region was attempted,[21,22] the "Raman" D and G showed a different or even opposite trend to the "IR" D and G peaks.[22,27] This again confirms that the IR spectra do not result from the activation of Raman modes. However, the apparent similarity between the Raman and IR spectra, in particular the presence of two main "peaks," can be explained as follows.

We have shown how IR probes the more delocalized sp^2 phase in N-free samples and the most delocalized and polarizable sp^2 phase in N-containing samples. On the other hand, a Raman spectrum at a given excitation energy weights those configurations resonant with that energy.[24] Thus Raman spectra excited with lower IR photons resonate with the most delocalized sp^2 phases, with the lowest gap. Therefore, in general terms, we can assume that the IR spectra and the Raman spectra excited in limit of low energy will probe the same sp^2 structures. In the Raman spectra the G peak is due to C-C stretching motions, whilst the D peak is due to breathing modes.[25,84] We can thus assume that the 1550–1600 IR band mainly has a stretching character and the $\sim$1250–1350 cm^{-1} has also a bending character. In detail, the selection rules for the modes contributing to IR and Raman spectra differ, but the overall spectrum shapes can appear roughly similar, after allowing for the appropriate weighting factors. A closer similarity between IR and Raman spectra can be expected for low sp^3 disordered carbons that show minimal peak dispersion with excitation energy,[21,24] in contrary to high sp^3 ta-C,[24] as confirmed by Fig. 12.
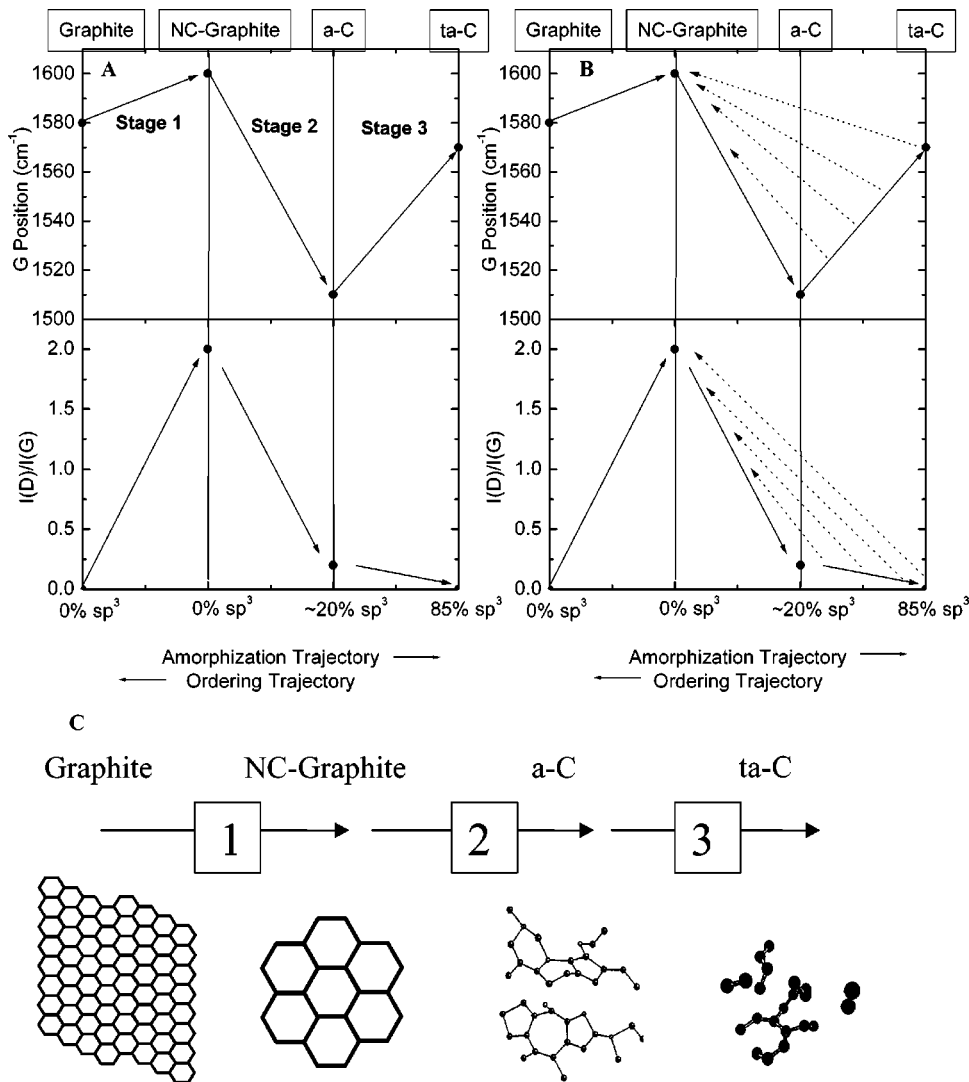
FIG. 13. Three-stage model of the variation of the Raman G position and the D to G intensity ratio $I(D)/I(G)$ with increasing disorder (Ref. 25). The dotted left-pointing arrows in (b) mark the nonuniqueness region in the ordering trajectory. (c) Shows the variation of the sp^2 configuration in the three amorphization stages.

VI. RAMAN SPECTRA OF CARBON SYSTEMS

Before analyzing in detail the Raman spectra of amorphous carbon nitrides, we first summarize the Raman spectra of nitrogen-free amorphous carbons. All carbons show common features in their Raman spectra in the 800–2000 cm^{-1} region, the so-called G and D peaks, which lie at around 1560 and 1360 cm^{-1} respectively for visible excitation, and the T peak at around 1060 cm^{-1}, seen only in UV excitation. Except for UV excitation, the Raman spectra are dominated by the sp^2 sites because the excitation resonates with π states. The G and D peaks are due to sp^2 sites. The G peak is due to the bond stretching of all pairs of sp^2 atoms in both rings and chains. The D peak is due to the breathing modes of sp^2 atoms in rings.[25,84,85] The T peak is due to the C-C sp^3 vibrations.[24]

We found that the Raman spectra of all carbons follow a three-stage model of increasing disorder,[24,25] Fig. 13(a). As we pass from ordered graphite to nanocrystalline graphite, to amorphous carbon and finally to sp^3 bonded ta-C, the sp^2 groups become first smaller, then topologically disordered and finally change from ring to chain configurations, as shown in Fig. 13(c). The G peak in visible excitation and the

intensity ratio of the D to G peak, $I(D)/I(G)$, vary as shown in Fig. 13(a). The full width at half maximum (FWMH) of the G peak decreases continuously as the disorder increases[86–89] (Fig. 14).

The Raman peaks shift with photon excitation energy, and this allows us to gain much more information on the sp^2 configuration. We concentrate on the G peak. Its position increases as the excitation wavelength decreases, from IR to UV, as show in Fig. 15. The dispersion rate increases with disorder. The G peak does not disperse in graphite itself, nanocrystalline (nc) graphite or glassy carbon.[24,90] The G peak only disperses in more disordered carbons, where the dispersion is proportional to the degree of disorder. The G peak dispersion separates the materials into two types. In materials with only sp^2 rings, the G peak dispersion saturates at a maximum of $\sim$1600 cm^{-1}, the G position in nc graphite. In contrast, in those materials also containing sp^2 chains, particularly ta-C and ta-C:H, the G peak continues to rise past 1600 cm^{-1} and can reach 1690 cm^{-1} at 229 nm excitation in ta-C. Thus, ta-C has the largest dispersion, followed by ta-C:H and polymeric a-C:H.

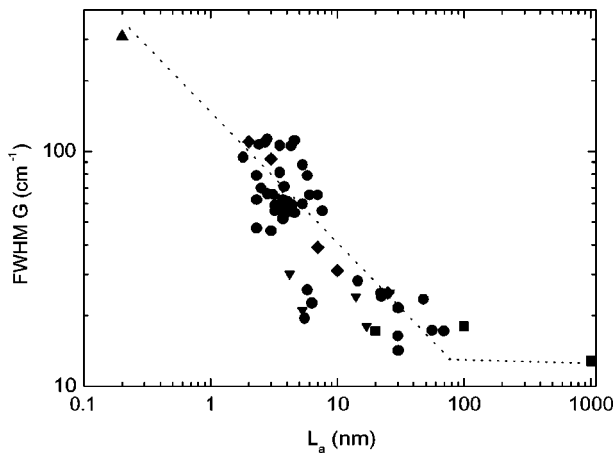A simplified interpretation of the Raman spectra is pos-

FIG. 14. Variation of G peak FWHM with decreasing sp^2 grain size L_a for visible excitation. (▲) Ferrari et $al.$ (Ref. 25), (●) Cuesta et $al.$ (Ref. 86), (◆) Lespade et $al.$ (Ref. 87), (■) Wilhelm et $al.$ (Ref. 88), (▼) Wang et $al.$ (Ref. 89). The line is a guide to the eye. The FWHMG saturates at ~ 12 cm^{-1} for high grain size graphitic samples.

sible if the sp^2 configuration depends in a unique fashion on the sp^3 content. This is the simplest case and sometimes happens for a-C, ta-C, or a-C:H deposited at room temperature. In this case, the Raman spectra depend uniquely on the sp^3 content, and thereby on the deposition parameters.[24,25]

However, under other circumstances, such as if the deposition temperature is varied or if the films are thermally annealed, the sp^2 configuration is not unique and it can vary independently of the sp^3 content. In this case, for a particular sp^3 content and excitation energy, we can have a number of
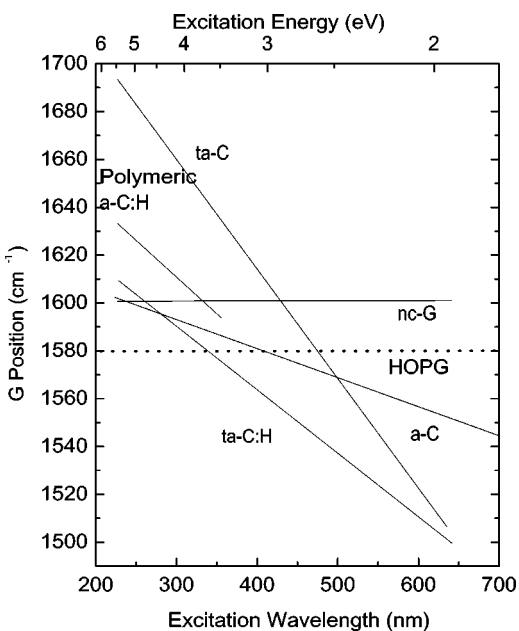

FIG. 15. Dispersion of G peak position with excitation wavelength (bottom scale) and excitation energy (upper scale), for HOPG, nc-G, ta-C, ta-C:H sp^2 a-C and polymeric a-C:H (Ref. 24).

different Raman spectra or, equivalently, similar Raman spectra for different sp^3 contents. This nonuniqueness is shown in the scheme of Fig. 13(b), where the ordering trajectory from ta-C towards nc graphite does not necessarily follow in reverse the same trajectory of the amorphization process,[25] as indicated by the dotted left-pointing arrows in Fig. 13(b). In this case a single wavelength study, particularly at visible excitation, cannot resolve this problem. The problem of nonuniqueness can be resolved by taking Raman spectra at different wavelengths, because each class of sp^2 configurations has different degrees of dispersion,[24] Fig. 15. In fact, due to the linear dispersion of the G peak with excitation wavelength,[24] it is sufficient to measure spectra at visible and UV (244 nm) excitation.

VII. RAMAN SPECTRA OF CARBON NITRIDES

We now consider the effect of nitrogen on the Raman spectra. The vibration frequencies of solid carbon nitrides are expected to lie close to the modes of the analogous unsaturated CN molecules, which are 1500–1600 cm^{-1} for chainlike molecules and 1300–1600 cm^{-1} for ringlike molecules.[79,91] This means that there is little distinction in the G-D region between modes due to C or N atoms. For example, the frequency of bond-stretching skeletal and ring modes is very similar in benzene, pyridine, and pyrrole, so it is difficult to assess if an aromatic ring contains nitrogen or not. The modes in amorphous carbon nitrides are also delocalized over both carbon and nitrogen sites because of nitrogen's tendency to promote more clustered sp^2 bonding. We therefore expect little difference between the Raman spectra of nitrogenated and N-free carbon films in the 1000–2000 cm^{-1} region. Indeed, we found no shift in the Raman spectra of two sputtered CN samples, one with ~ 26 at. % ^{14}N and the other with the same content of ^{15}N. On the other hand, we clearly expect to detect a direct contribution of CN sp^1 bonds only in the 2200 cm^{-1} region.

The similarity of vibrational frequencies of C-C and C-N modes could make the interpretation of the skeletal modes quite difficult, if we were hoping to find C-N and N-N modes, as in some previous work.[35–38] However, we neglect the direct contributions of C-N or N-N bonds to the spectra,[23] unless there is a clear reason for them, for example, from isotopic substitution. Instead, we analyze the trends in the G and D positions in the same way as in N-free samples. This will enable us to explain the observed spectra in the 1000–2000 cm^{-1} region, without needing to invoke heteropolar modes. On the other hand, UV Raman can detect CN sp^1 vibrations even when not seen in visible Raman, due to the resonant enhancement.

VIII. DETAILED RESONANT RAMAN SPECTRA OF CARBON NITRIDES

The samples used for Raman measurements are deposited on Si substrates. We consider each of the four classes of carbon nitrides. Figure 16 shows the Raman spectra excited at 244, 325, and 514 nm of a a-C:N film with 33% N content and $\sim 33\%$ sp^3 bonding. This film was deposited by a com-
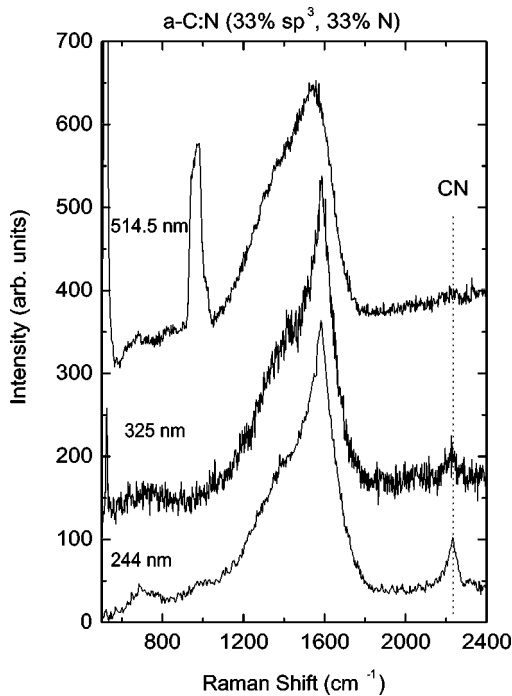
FIG. 16. Multiwavelength Raman spectra of a 33% sp^3, 33% N a-C:N. For 514.5 nm and, to a lesser extent, 325 nm excitations the contributions of the substrate Si Raman peaks at ~521 and 970 cm^{-1} are also seen.

bination of a FCVA providing C ions and an ECWR source providing N ions and it is one of a series of $(t)a$-C:N films of increasing N content.[12] We then examined the whole series of $(t)a$-C:N films deposited either by introducing a N_2 background gas into the FCVA (Refs. 29, and 49) or by a dual ion beam-plasma beam source comprising a FCVA and an ECWR.[12] The N vs sp^3 relation for carbon nitrides is shown in Fig. 3. Although there is a general decrease of sp^3 content for increasing N content, the precise variation depends on the deposition system. This implies that the sp^2 content and sp^2 clustering is not unique for a given N content. Thus, the dependence of the optical gap on N content does not follow that of the sp^3 content, as seen in Fig. 4.

The Raman spectra were measured in backscattering configuration on a range of Renishaw micro-Raman spectrometers optimised for visible and UV excitation and care was taken to avoid any damage, as previously described.[24,25] The spectra were then analyzed by fitting a Lorentzian to the D peak and any T peak and a Breit-Wigner-Fano (BWF) line shape to the G peak. The G peak position corresponds to the maximum of the BWF, rather than its center. The details of the fitting procedure are discussed in Ref. 25. Figures 17–22 compare how various parameters vary for these ta-C:N films as a function of N content.

Figure 17(a) shows the variation of G peak position with N content, for 244 and 514 nm excitation. The G peak remains roughly constant with increasing N content for 514 nm excitation, whereas it falls sharply with N content for 244 nm excitation, from 1665 to 1590 cm^{-1}. This indicates that N addition has replaced the C=C olefinic groups with aro-
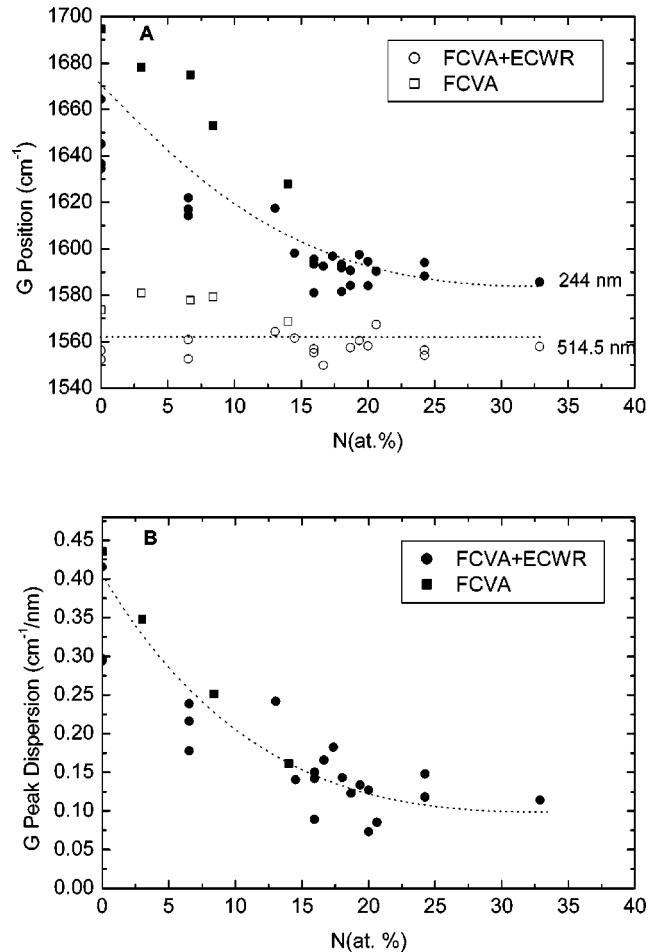

FIG. 17. (a) G peak position versus N content for 244 and 514 nm excitation for $(t)a$-C:N samples deposited by FCVA+ECWR and FCVA alone. (b) Dispersion of G peak versus N content. The lines are guides to the eye.
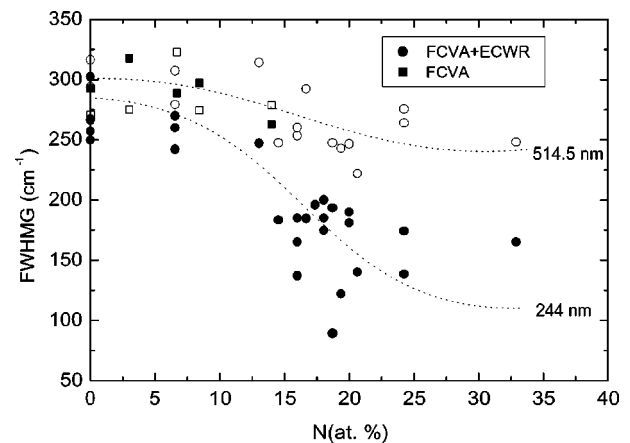

FIG. 18. Variation of G peak FWHM with N content for $(t)a$-C:N films. Circles represent samples deposited by FCVA +ECWR and squares samples deposited by FCVA only. Open symbols refer to 514.5 nm excitation, full symbols refer to 244 nm excitation. The lines are guides to the eye.
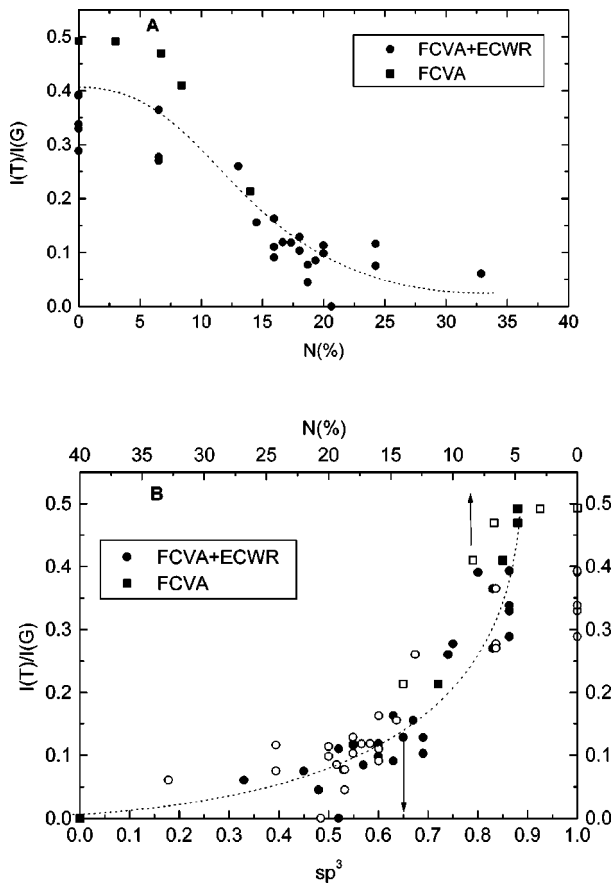
FIG. 19. (a) Variation of T to G peak intensity ratio $I(T)/I(G)$ with N content for $(t)a$-C:N films. (b) Variation against sp^3 content, lower scale, and N content, upper scale and open symbols. The lines are guides to the eye.

FIG. 20. (a) Variation of D to G peak intensity ratio $I(D)/I(G)$ with N content for $(t)a$-C:N films. (b) Plot of $I(D)/I(G)$ against $1/(\text{gap})^2$. Circles represent samples deposited by FCVA+ECWR and squares samples deposited by FCVA only. Open symbols refer to 514.5 nm excitation, full symbols refer to 244 nm excitation. The lines are guides to the eye.

matic groups. The G peak position varies roughly linearly with excitation wavelength.[24] Figure 17(b) plots the dispersion (slope) of the G peak wave number with excitation wavelength against the N content. The dispersion falls sharply up to 15% N, and then declines gradually until it reaches a constant value above 25% N.

Figure 18 shows the variation of the full width at half maximum (FWHM) of the G peak with N content. The G peak width indicates the bond angle distortions in the configurations excited. The G peak is always narrower for UV (244 nm) excitation than for visible excitation because a smaller range of sp^2 configurations is probed at UV. The G width is seen to decrease with increasing N content, and much more strongly for UV excitation but rather weakly for visible excitation. This indicates a substantial loss of disorder of small clusters for higher N content.

The T peak is due to sp^3 sites. Figure 19(a) shows the variation of the T to G peak ratio $I(T)/I(G)$ with N content. The $I(T)/I(G)$ ratio decreases sharply in the range 10–15% showing that there is a sizable loss of sp^3 bonding. The variation of $I(T)/I(G)$ here is similar to that in the base case of ta-C.[24] Figure 19(b) shows the variation plotted against sp^3 content. This is converted into a variation with N content, along the top scale, using the roughly linear dependence of sp^3 fraction on N content for these films [Fig. 21(a)].
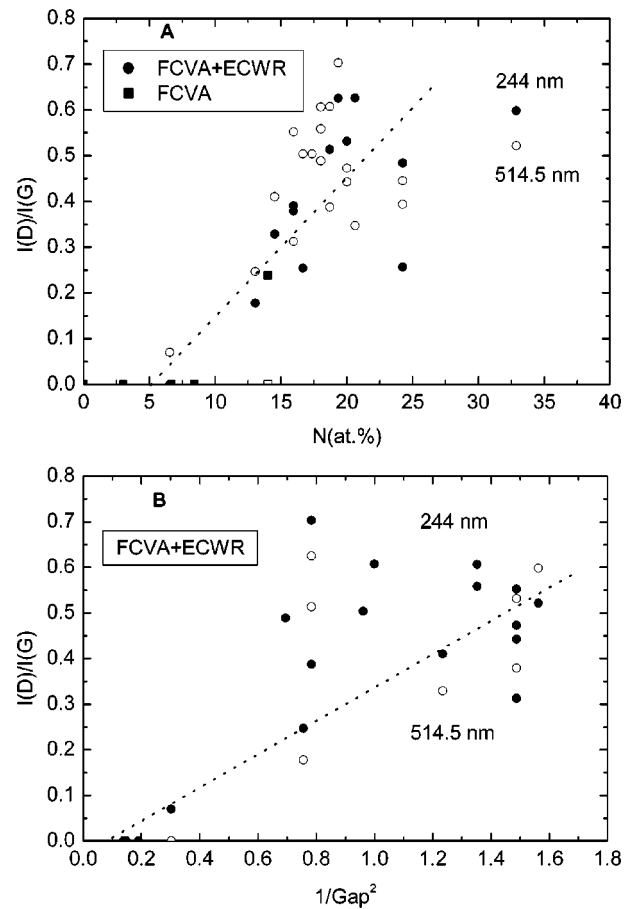
A major effect of N introduction is to increase the clustering of the sp^2 phase, which is indicated by the D peak. Figure 20(a) shows the variation of the D to G intensity ratio $I(D)/I(G)$ for both UV and visible excitation. The $I(D)/I(G)$ ratio is similar for both excitations. $I(D)/I(G)$ increases substantially above 5% N content.

The fact that in these films the sp^3 content varies linearly with N, as shown in Fig. 21(a), does not necessarily imply that the sp^2 clustering varies in a similar way. Indeed, the variation of clustering with sp^2 fraction is not fixed. The cluster diameter L_a can be inferred from the optical gap. Figure 21(b) shows that the decay of optical gap with increasing sp^2 content for these ta-C:N is more nonlinear than in other $(t)a$-C:(H) films.[92] The $I(D)/I(G)$ ratio increases as the introduction of N causes the sp^2 clusters to become larger. $I(D)/I(G)$ is expected to increase as the cluster diameter L_a squared.[25] As the band gap varies inversely with L_a, then this gives a variation of $I(D)/I(G)$ with $1/(\text{optical gap})^2$.[25] Figure 20(b) plots $I(D)/I(G)$ against $1/\text{gap}^2$ to test this dependence. A fair but very scattered fit is found. This, however, confirms that the fundamental dependence of $I(D)/I(G)$ is on sp^2 clustering and thereby on band
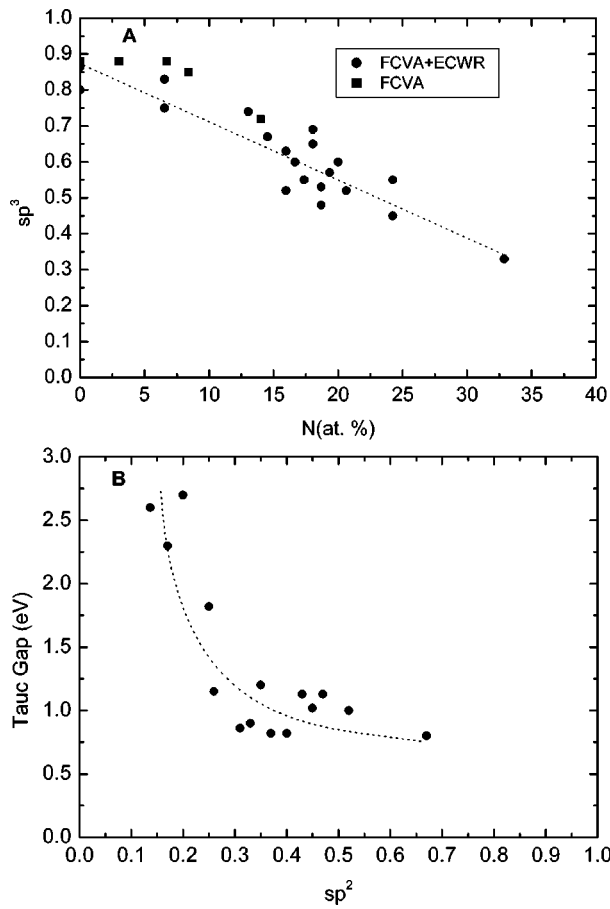
FIG. 21. (a) sp^3 content vs N content and (b) Optical gap vs sp^2 content for $(t)a$-C:N films (Refs. 23, 12, 49). The lines are guides to the eye.
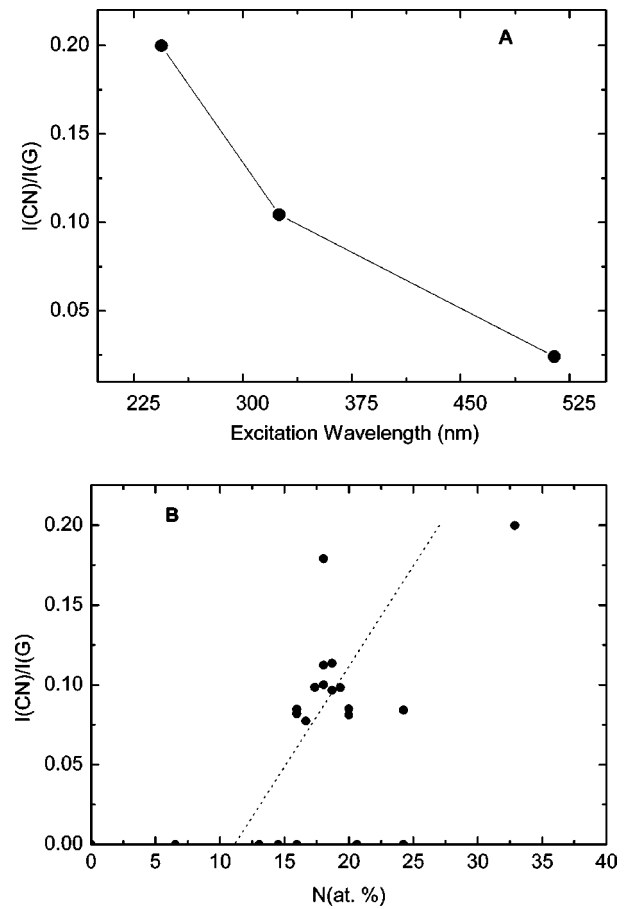

FIG. 22. (a) Variation of CN peak to G peak intensity ratio $I(\text{CN})/I(G)$ with excitation wavelength for the sample of Fig. 16. (b) Variation of $I(\text{CN})/I(G)$ with N content, measured at 244 nm; the dotted line is a guide to the eye.

gap. It depends only indirectly on the sp^2 fraction itself, as expected from the different trends of gap on sp^2 fraction as a function of N content, Fig. 21.

sp^1 bonded CN groups give rise to stretching modes around 2200 cm^{-1}. These CN groups are detrimental to hardness of a-C:N as they are terminating groups, which lower the network connectivity. The groups are seen in IR spectra and are seen weakly in visible Raman at 514 nm. Figure 16 shows that the 2200 cm^{-1} mode is clearly seen for 244 nm excitation, while it was barely detectable for 514 nm excitation. The mode's intensity increases by an order of magnitude, as the excitation changes from 514 to 244 nm, as shown in Fig. 22(a).

The enhancement of sp^1 CN groups in UV excitation occurs because this group has a π-π^* band gap of 5–6 eV. The gap is relatively constant, it does not display the wide range of local gaps found for sp^2 bonded groups, so it is resonant for UV excitation.

Figure 22(b) shows a roughly linear increase of $I(\text{CN})/I(G)$ ratio with increasing N content, beyond a threshold N content of ~10%. A similar trend is observed for all carbon nitrides, as discussed later. However, the trend is stronger and better defined for hydrogenated carbon nitride films. This shows that N is less likely to form sp^1 sites in ta-C:N than in the softer materials.[93,94] This is indicated by

the 10–12% N content threshold, below which no CN peak is seen. Note that some films with a high 20–25% N content have no significant CN peak even for UV excitation in Fig. 22(b). This must be related to the specific deposition conditions, which we do not discuss here, as we focus on general trends.

Figures 23–29 show a similar set of data for a series of $(t)a$-C:H:N films deposited by a N$_2$/C$_2$H$_2$ plasma from an ECWR source.[23] Figure 24 summarizes the variation of the sp^3 content and the optical gap with N content for these films. The sp^3 content falls significantly above 20% nitrogen, and the gap rises, as the films become "polymeric."[23]

As for the ta-C:N case, the combination of visible and UV excitation allows a much better analysis of the trends. Figure 23 shows the multiwavelength Raman spectra for a representative ta-C:H:N film. The variation of the G peak position is shown in Fig. 25(a). The G peak position decreases with N content for UV excitation from 1620 to 1600 cm^{-1}, and it goes up for visible excitation. These data are combined into the variation of G peak dispersion, and its variation with N content is shown in Fig. 25(b). The dispersion falls almost linearly with N content. This shows that the sp^2 sites have become ordered in a more aromatic fashion for higher N contents.
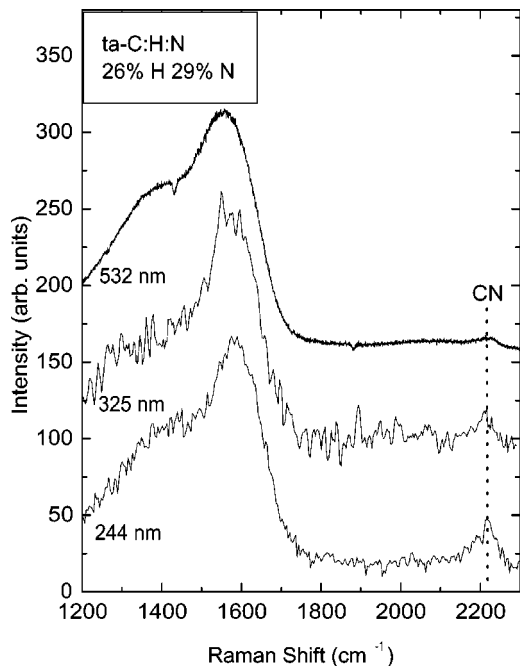
FIG. 23. Multiwavelength Raman spectra of a ta-C:H:N film with ~26% H and 29% N, deposited by ECWR.

Figure 26 shows that the G peak FWHM decreases with increasing N content, for both UV and visible excitations. The G width is smaller for UV excitation as usual. This indicates that the sp^2 configurations become more ordered at high N contents.

The T peak in ta-C:H reflects only the C—C sp^3 bonded component.[24] Figure 27(a) shows the variation of $I(T)/I(G)$ ratio for $(t)a$-C:H:N films plotted against N content. The T peak intensity shows a sharp drop at 20% N content, corresponding to the transition from dense network to polymeric network in Fig. 24. The $I(T)/I(G)$ ratio is seen to increase linearly with sp^3 content when plotted in Fig. 27(b). In general the T peak intensity is smaller in $(t)a$-C:H than in H-free films with the same overall sp^3 content and sp^2 clustering.[24] This explains why the trends of $I(T)/I(G)$ vs N or sp^3 are better defined in $(t)a$-C:N. However, the trends of

FIG. 25. (a) Variation of G peak position with N content at 244 and 514 nm excitation for $(t)a$-C:H:N films. (b) variation of G peak dispersion with N content. The lines are guides to the eye.

all other parameters are better defined in $(t)a$-C:H:N, more than compensating the poorer $I(T)/I(G)$ data.

Figure 28(a) shows the variation of $I(D)/I(G)$ ratio with N content. The ratio varies as (optical gap)$^{-2}$ again, with an offset,[25,95] as shown in Fig. 28(b) and the trend is much clearer than in Fig. 20(b).

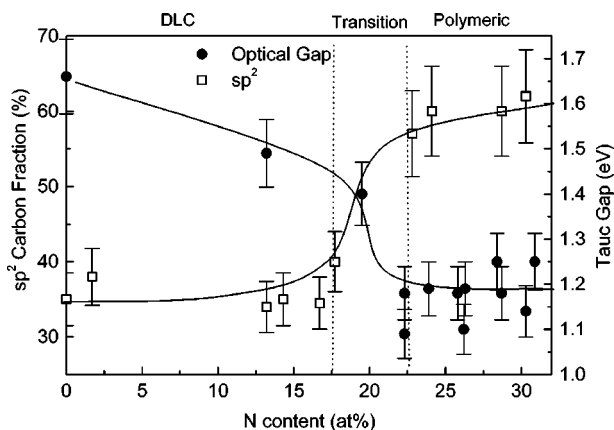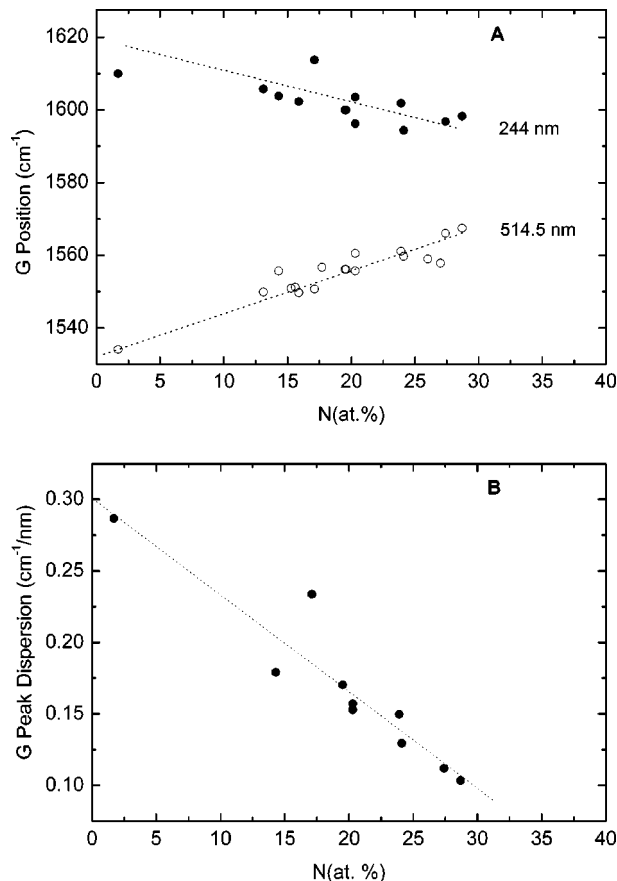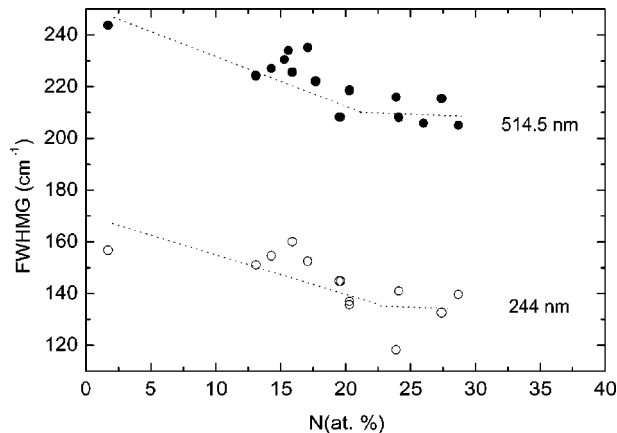Figure 29 shows the variation in the intensity of the CN

FIG. 24. Variation of sp^3 fraction and optical gap with N content for ta-C:H:N (Ref. 23). The lines are guides to the eye.

FIG. 26. Variation of G peak FWHM with N content for $(t)a$-C:H:N films at 244 and 514 nm excitation. The lines are guides to the eye.
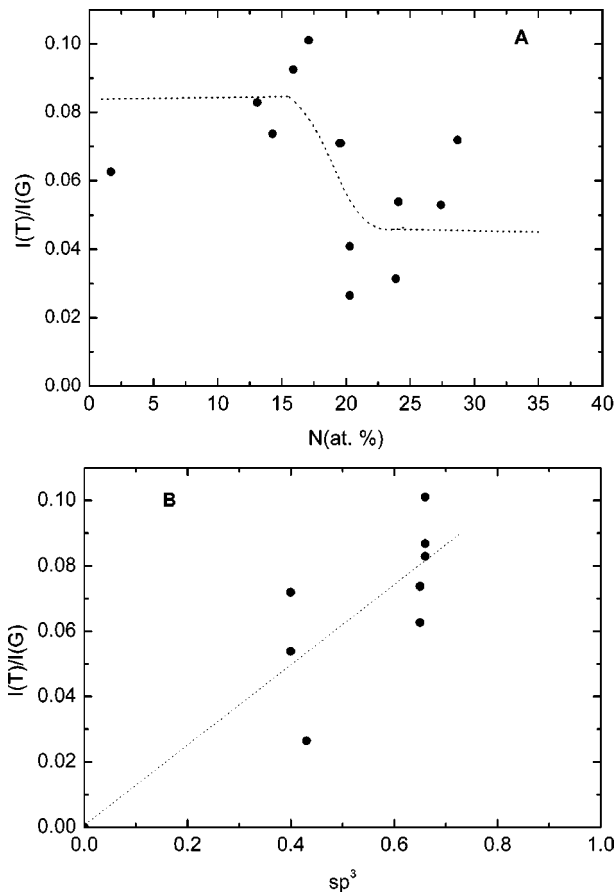
FIG. 27. (a) Variation of T to G peak intensity ratio $I(T)/I(G)$ with N content for $(t)a$-C:H:N films. (b) Variation of $I(T)/I(G)$ versus sp^3 content. The lines are guides to the eye.
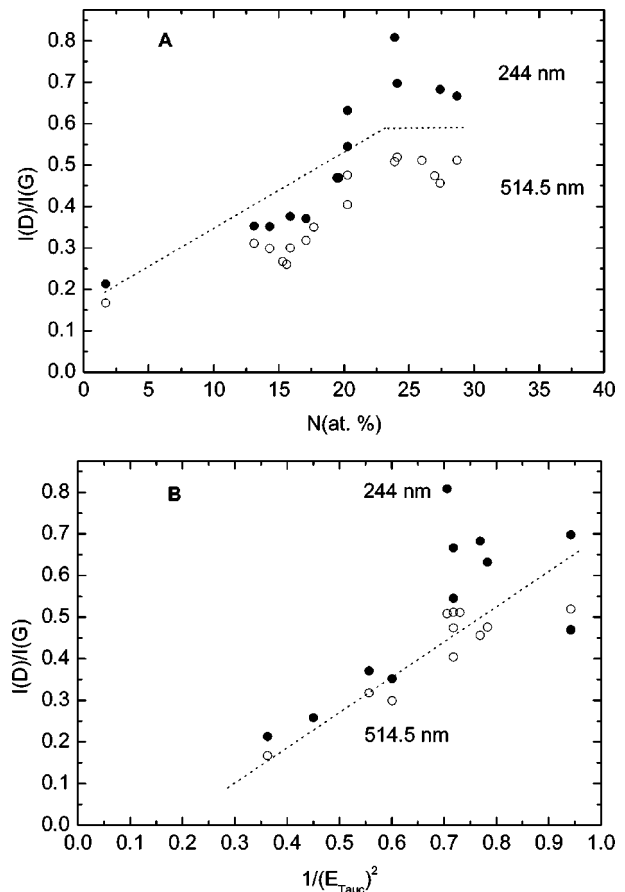

FIG. 28. (a) Variation of D to G peak intensity ratio $I(D)/I(G)$ with N content for $(t)a$-C:H:N films. (b) Plot of $I(D)/I(G)$ against $1/(\text{gap})^2$. Open symbols refer to 514.5 nm excitation, full symbols refer to 244 nm excitation. The lines are guides to the eye.

sp^1 mode. The mode's intensity increases by an order of magnitude as the excitation changes from 514 to 244 nm, as shown in Fig. 29(a), similar to that in $(t)a$-C:N, Fig. 22(a). However, the intensity is higher than in ta-C:N, and there is now a clearer linear dependence of $I(\text{CN})/I(G)$ on N content, Fig. 29(b). All nitrogen-containing $(t)a$-C:H films show a CN mode, unlike ta-C:N where some films did not.

We finally consider a-C:N films prepared by magnetron sputtering at 200 °C with a deposition system as described by Wienss *et al.*[28] The Raman spectra for excitation at 244 and 514 nm are shown in Fig. 30 for a film with 10% N content. These films are predominantly sp^2 bonded, and their Raman spectra show a differ behavior to those of $(t)a$-C:N and $(t)a$-C:H:N discussed so far.

Figure 31(a) shows the variation of G peak position for visible and UV excitation with N content. The G peak moves downwards in both cases, but now the fall for visible excitation is greater. Recall that in $(t)a$-C:N, the G peak was almost constant for visible excitation, Fig. 17(a), while it moved up in $(t)a$-C:H:N, Fig. 25(a). Figure 31(b) shows the G peak dispersion against N content. The dispersion increases with N content, whereas for the previous $(t)a$-C:N and $(t)a$-C:H:N it decreased, Figs. 17(b), 25(b). The increase is because N is introducing *disorder* into the sp^2 sites, whereas in tetrahedral materials N was inducing sp^2 order-

ing. This is further demonstrated by Fig. 32, which shows the G peak FWHM increasing with increasing N content. This again indicates how disorder is increasing as N is added.

Figure 33 shows the variation of $I(\text{CN})/I(G)$ as detected in UV Raman as a function of the N content. Also in this case, the 514 nm Raman spectra do not provide enough CN sp^1 intensity for the peak to be properly fitted. Comparing the CN intensities of Figs. 33, 29(b), and 22(b), we see that more CN groups are present for the same N content in sputtered a-C:N than in ta-C:H:N and considerably more than in ta-C:N. As in $(t)a$-C:N and, to a lesser extent in $(t)a$-C:H:N, the $I(\text{CN})/I(G)$ vs N relation is slightly nonlinear, with a threshold N content for CN sp^1 bonds to be formed.

Note that for sputtered CN films, each Raman parameter shows a relatively small variation with N. For example, in Fig. 31(a) the G peak downshifts only 5 cm^{-1} in UV Raman and $\sim$15 cm^{-1} for 514 nm Raman. This differs from the large variation of these parameters in Figs. 17, and 25. The trends of Fig. 31(a), for a single excitation wavelength, are just a few wave numbers above the instrument resolution. However, the combination of visible and UV excitation definitely validates them and gives a clearer analysis, as further discussed in Sec. IX.
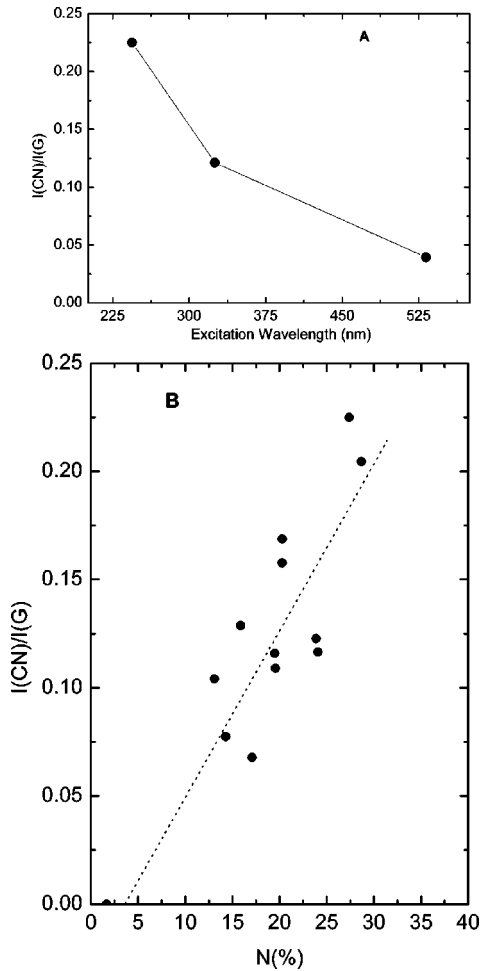
FIG. 29. (a) Variation of CN peak to G peak intensity ratio $I(CN)/I(G)$ with excitation wavelength for the ta-C:H:N sample of Fig. 23. (b) Variation of $I(CN)/I(G)$ with N content, measured at 244 nm. The dotted line is a guide to the eye.

IX. THREE STAGE MODEL FOR RESONANT RAMAN SPECTRA OF CARBON NITRIDES

We can thus now fully extend the three-stage model for multiwavelength excitation[24] to explain the trends in the Raman parameters in any carbon nitride measured at any excitation wavelength. In particular, we will consider the trends in the G peak position, as summarized in Fig. 34.

We recall that, in general, adding N causes an independent evolution of the sp^3 fraction and sp^2 clustering. This causes a nonuniqueness of sp^2 configuration for a given sp^3 content.[24,25] This means that the ordering trajectory resulting by adding N to ta-C or ta-C:H is not equivalent to the reverse of the amorphization trajectory leading from a-C to ta-C. Thus, for a certain sp^3 content, we can have various G peak positions, both in visible and UV excitation. This effect is summarized for visible excitation in Fig. 13(b), by the triangular regions defined by the dotted arrows pointing in the ordering direction. These indicate the various G peak positions and $I(D)/I(G)$ ratios that could correspond to a given sp^3 content. Figure 34 plots the schematic variation of G peak position for 244 and 514 nm excitation in carbon
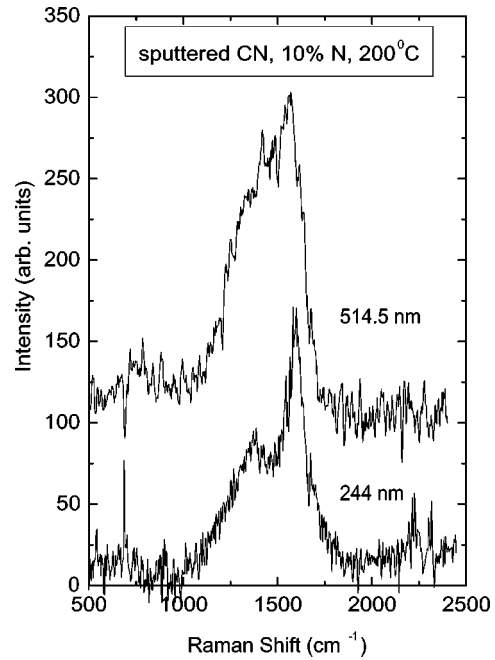

FIG. 30. Multiwavelength Raman spectra of a sputtered a-C:N, deposited at $\sim$200 °C with $\sim$10% N (Ref. 28).

nitrides. The triangular shaped region representing the nonuniqueness for visible excitation becomes a "bow-tie" shaped region for 244 nm, as defined in Fig. 34.[24] The direction of the arrows indicates if we are following an amorphization trajectory (from left to right, defined by the bold arrows in
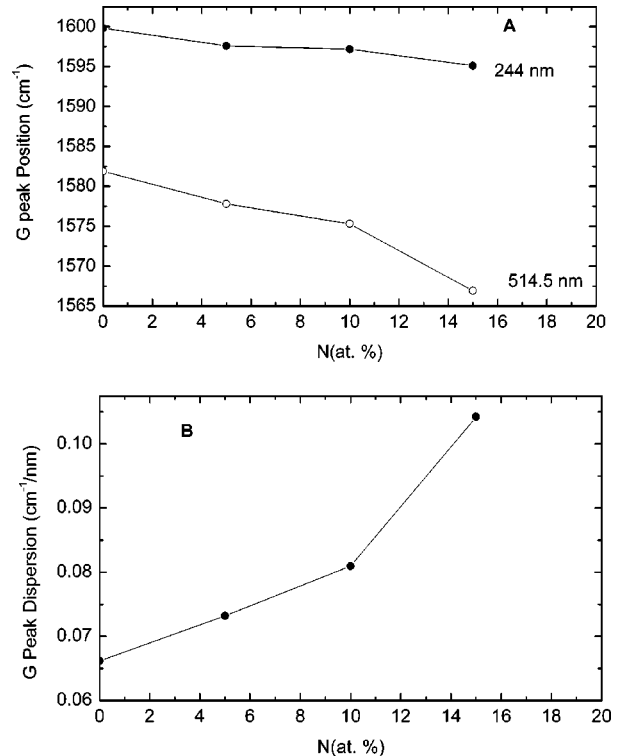

FIG. 31. (a) Variation of G peak position with N content for 244 and 514 nm excitation for high-temperature deposited sputtered a-C:N films. (b) Variation of G peak dispersion with N content.
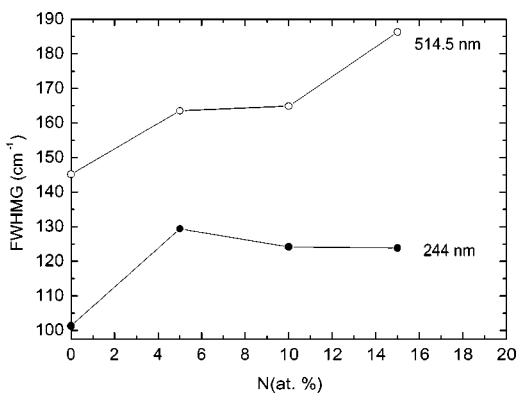
FIG. 32. Variation of G peak FWHM with N content for 244 and 514 nm excitation for high-temperature deposited sputtered a-C:N films.

Fig. 34) or an ordering trajectory, from right to left (defined by the left-pointing continuous arrows in Fig. 34). The nonuniqueness regions are defined by the dotted, left-pointing, arrows in Figs. 34 and 13(b).

Figure 34 immediately explains the trends for $(t)a$-C:N and $(t)a$-C:H:N. Clustering in UV Raman causes a G peak downshift with increasing N content for stage 3 carbons. As explained above, clustering means following the ordering trajectory in Fig. 34. The downshift is larger for higher initial G peak positions above 1600 cm^{-1}, the band limit for graphite. On the contrary, clustering raises the G peak for visible excitation. This upshift is larger the lower the initial G peak position. Thus, following the ordering trajectory, the G peak trends for UV and visible excitation are *opposite* for stage 3 carbons. This is what is seen in Figs. 17(a) and 25(a), and is predicted by Fig. 34. Furthermore, this *trend inversion*, between visible and UV Raman, causes a G peak dispersion that is higher for lower sp^2 clustering, i.e., for lower N content in carbon nitrides. Again, this prediction of Fig. 34 is seen experimentally in Figs. 17(b) and 25(b). The G peak dispersion thus allows us to resolve the ambiguity that nonuniqueness can cause for single excitation energy measurements, especially in the visible, as seen, e.g., in Fig. 17(a), where there is almost no variation of G peak position with N
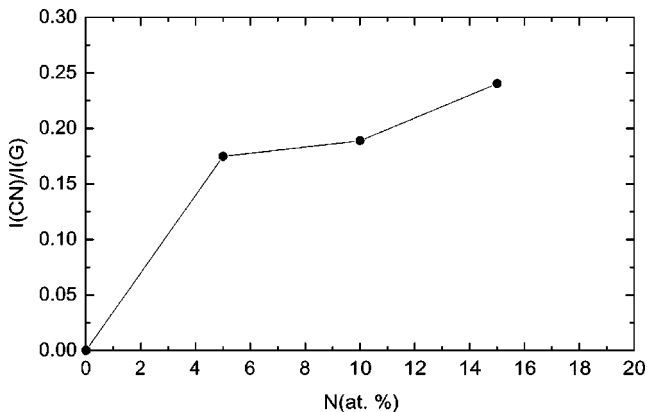

FIG. 33. Variation of CN peak to G peak intensity ratio $I(\text{CN})/I(G)$ with N content, measured at 244 nm for high-temperature deposited sputtered a-C:N films.
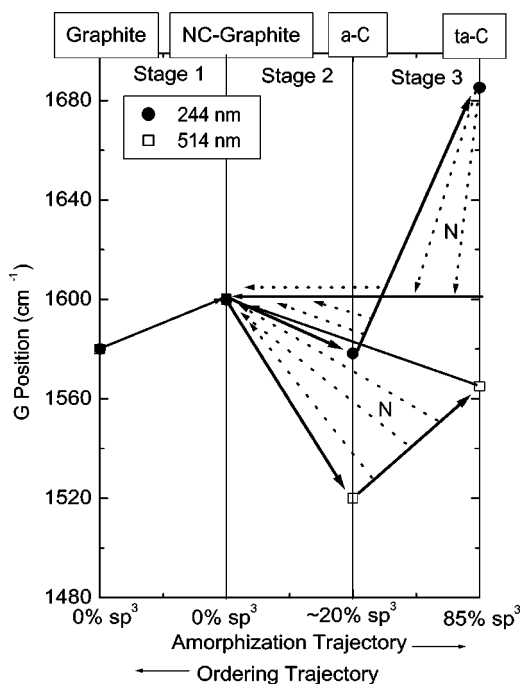

FIG. 34. Three stage model of the variation of the G peak position versus disorder for visible and UV excitation in amorphous carbon nitrides. The bold right-pointing arrows represent the amorphization trajectory is stages 2 and 3. The "bow-tie" and triangular-shaped regions defined by the dotted and continuous left-pointing arrows define the nonuniqueness regions for UV and visible excitations respectively. N introduction generally induces nonuniqueness in stage 3, as indicated by the letter N in the graph.

content at 514 nm. This implies that the G peak dispersion is the main parameter to be linked with N content, or sp^2 fraction, as indeed shown by its well-defined trends in Figs. 17 and 25.

It has been noted how nitrogen addition in a-C may increase its hardness and elastic recovery, especially at temperatures higher than 150 °C.[4,28,41,96] In that case, N does not cause more clustering of sp^2 sites, but more cross-linking and thus increased disorder,[4,93] even though not necessarily through a significant sp^3 increase.[96] We thus expect a relation between sp^3 content and sp^2 configuration with increasing N content, since the decrease of sp^2 clustering means that we are following the amorphization trajectory. This is the case of the sputtered carbon nitrides of Figs. 30–33. They can be classified as stage 2 carbons with increasing amorphization. From Fig. 34, we see that the amorphization trajectory for stage 2 carbons predicts a decrease of G peak position for both visible and UV Raman spectra (bold right-pointing arrows). Figure 34 also predicts a larger decrease for 514 nm excitation. This implies that the G peak dispersion must increase for increasing N content, as is indeed experimentally seen, Fig. 31(b).

In general, we can find cases where N induces clustering also in stage 2 carbons, e.g., for low-temperature depositions. In this case, Fig. 34 predicts a rise of G position in the visible and *also* for UV excitation (dotted right-pointing arrows). There is no more the trend inversion typical of stage 3 carbons. However, the raise of G with N for UV excitation is

lower than the corresponding raise for visible excitation, as shown in Fig. 34. Thus, even without trend inversion, this again would result in a lower G peak dispersion with increasing N content. Thus for *any* carbon, a lower G peak dispersion *always* means ordering and vice versa an increase of G peak dispersion *always* means disordering. This again shows that the G peak dispersion is the simplest, most direct way to characterize amorphous carbon nitride films in terms of N content, gap, sp^2, or sp^3 content, or hardness and density.

Finally, we stress how Fig. 34 is not a fit to experimental data, but a predictive scheme. It is derived form the general model of the G peak evolution in N-free samples[24,25] outlined in Sec. VI. The difference is that now the nonuniqueness is induced by N rather than by other factors such as annealing. Thus, all the Raman experimental trends reported above could be predicted by Fig. 34. Indeed the increase of the G peak dispersion in high-temperature sputtered a-C:N, where N induces disorder, is a most definitive proof that the three stage model works for carbon nitrides. This is also the first time that Raman spectroscopy gives direct evidence of the unusual structural evolution induced by N in high-T sputtered a-C:N.[4,28,41,96]

X. CONCLUSIONS

We classified amorphous carbon nitride films in four classes, according to the corresponding N-free film: a-C:N, a-C:H:N, ta-C:H:N, and ta-C:N. We presented a general model able to explain the IR intensities in the 800–2000 cm^{-1} spectral region in carbon films, with and without nitrogen. For amorphous carbon nitrides we showed that the IR bands are never directly due to CN, NN, and NH vibrations, but their intensity is related to the N content due to the po-larization of the sp^2 phase induced by the terminal N atoms.

We showed how the Raman spectra taken at any excitation energy can be explained in terms of an a-C based model, without need of extra peaks due to CN, NN, or NH modes. We analyzed a wide variety of samples for the four classes and presented the Raman spectra as a function of N content, sp^3 content, and band gap. In highly sp^3 samples such as ta-C or ta-C:H, nitrogen increases the clustering of the sp^2 phase and worsens the mechanical properties. This is reflected in a decrease of the G peak dispersion. On the other hand, in sp^2-rich sputtered carbon nitride films, nitrogen tends to decrease the clustering and so increase the G peak dispersion. In all cases, a multiwavelength study allows a direct correlation of the Raman parameters with the N content, which is not generally possible for single wavelength excitation. The G peak dispersion emerges as a most informative parameter for Raman analysis. UV Raman enhances the sp^1 CN peak, which is usually too faint to be seen in visible excitation. As for N-free samples, UV Raman also enhances the C-C sp^3 bonds vibrations, allowing the sp^3 content to be quantified.

ACKNOWLEDGMENTS

---

*Email address: acf26@eng.cam.ac.uk

[1] A. Y. Liu and M. L. Cohen, Science **245**, 841 (1989).

[2] S. Muhl and J. M. Mendez, Diamond Relat. Mater. **8**, 1809 (1999).

[3] A. Badzian, T. Badzian, R. Roy, and W. Drawl, Thin Solid Films **354**, 148 (1999).

[4] N. Hellgren, M. P. Johansson, E. Broitman, L. Hultman, and J. E. Sundgren, Phys. Rev. B **59**, 5162 (1999).

[5] E. C. Cutiongco, D. Li, Y. W. Chung, and C. S. Bhatia, J. Tribol. **118**, 543 (1996).

[6] J. Robertson, Thin Solid Films **383**, 81 (2001).

[7] C. Ronning, H. Feldermann, R. Merk, H. Hofsass, P. Reinke, and J. U. Thiele, Phys. Rev. B **58**, 2207 (1998).

[8] P. Hammer, N. M. Victoria, and F. Alvarez, J. Vac. Sci. Technol. A **16**, 2941 (1998).

[9] S. Souto, M. Pickholz, M. C. dos Santos, and F. Alvarez, Phys. Rev. B **57**, 2536 (1998).

[10] N. Hellgren, J. Guo, C. Sathe, A. Agui, J. Nordgren, Y. Luo, H. Agren, and J. E. Sundgren, Appl. Phys. Lett. **79**, 4348 (2001).

[11] J. M. Ripalda, E. Roman, N. Diaz, L. Galan, L. Montero, G. Comelli, A. Baraldi, S. Lizzit, A. Goldoni, and G. Paolucci, Phys. Rev. B **60**, 3705 (1999).

[12] S. E. Rodil, W. I. Milne, J. Robertson, and L. M. Brown, Appl. Phys. Lett. **77**, 1458 (2000).

[13] S. Waidmann, M. Knupfer, J. Fink, B. Kleinsorge, and J. Robertson, J. Appl. Phys. **89**, 3783 (2001).

[14] B. Dischler, Eur. Mater. Res. Soc. Symp. Proc. **17**, 189 (1987).

[15] J. Ristein, R. T. Stief, L. Ley, and W. Beyer, J. Appl. Phys. **84**, 3836 (1998).

[16] Y. Bounouh, M. L. Theye, A. Dehbi-Alaoui, A. Matthews, and J. P. Stoquert, Phys. Rev. B **51**, 9597 (1995).

[17] M. L. Theye, V. Paret, and A. Sadki, Diamond Relat. Mater. **10**, 182 (2001); V. Paret, Ph.D. thesis, Universite' Pierre et Marie Curie, 1999.

[18] J. H. Kaufman, S. Metin, and D. D. Saperstein, Phys. Rev. B **39**, 13 053 (1989).

[19] N. M. Victoria, P. Hammer, M. C. Dos Santos, and F. Alvarez, Phys. Rev. B **61**, 1083 (2000).

[20] F. Alvarez, N. M. Victoria, P. Hammer, F. L. Friere, and M. C. dos Santos, Appl. Phys. Lett. **73**, 1065 (1998).

[21] G. Fanchini, A. Tagliaferro, G. Messina, S. Santangelo, A. Paoletti, and A. Tucciarone, J. Appl. Phys. **91**, 1155 (2002); G. Fanchini, G. Messina, A. Paoletti, S. C. Ray, S. Santangelo, A. Tagliaferro, and A. Tucciarone, Surf. Coat. Technol. **151**, 257 (2001).

[22] J. M. Mendez, A. Gaona-Couto, S. Muhl, and S. Jimenez-Sandoval, J. Phys.: Condens. Matter **11**, 5225 (1999).

[23] S. E. Rodil, A. C. Ferrari, J. Robertson, and W. I. Milne, J. Appl. Phys. **89**, 5425 (2001).

[24] A. C. Ferrari and J. Robertson, Phys. Rev. B **64**, 075414 (2001).

[25] A. C. Ferrari and J. Robertson, Phys. Rev. B **61**, 14 095 (2000).

[26] S. R. P. Silva, J. Robertson, G. A. J. Amaratunga, B. Rafferty, L. M. Brown, D. F. Franceschini, and G. Mariotto, J. Appl. Phys. **81**, 2626 (1997).

[27] J. Schwan, V. Batori, S. Ulrich, H. Ehrhardt, and S. R. P. Silva, J. Appl. Phys. **84**, 2071 (1998).

[28] A. Wienss, G. Persch-Schuy, R. Hartmann, P. Joeris, and U. Hartmann, J. Vac. Sci. Technol. A **18**, 2023 (2000).

[29] M. C. Polo, J. L. Andujar, A. Hart, J. Robertson, and W. I. Milne, Diamond Relat. Mater. **9**, 663 (2000).

[30] G. Mariotto, F. L. Freire, and C. A. Achete, Thin Solid Films **241**, 255 (1994).

[31] J. R. Shi, X. Shi, Z. Sun, S. P. Lau, B. K. Tay, and H. S. Tan, Diamond Relat. Mater. **10**, 76 (2000); Thin Solid Films **366**, 169 (2000).

[32] Y. H. Chen, B. K. Tay, S. P. Lau, X. Shi, X. L. Qiao, J. G. Chen, Y. P. Wu, and C. S. Xie, Appl. Phys. A: Mater. Sci. Process. **73**, 341 (2001).

[33] Y. H. Cheng, B. K. Tay, S. P. Lau, X. Shi, X. L. Qiao, Z. H. Sun, J. G. Chen, Y. P. Wu, and C. S. Xie, Diamond Relat. Mater. **10**, 2137 (2001).

[34] A. C. Ferrari, Diamond Relat. Mater. **11**, 1053 (2002).

[35] M. R. Wixom, J. Am. Ceram. Soc. **73**, 1973 (1990).

[36] A. K. M. S. Chowdhury, D. C. Cameron, and M. S. J. Hashimi, Thin Solid Films **332**, 62 (1998).

[37] M. K. Fung, W. C. Chan, Z. Q. Gao, I. Bello, and S. T. Lee, Diamond Relat. Mater. **8**, 472 (1999).

[38] Y. K. Yap, S. Kida, T. Aoyama, Y. Mori, and T. Sasaki, Appl. Phys. Lett. **73**, 915 (1998).

[39] J. Robertson and C. A. Davis, Diamond Relat. Mater. **4**, 441 (1995).

[40] N. V. Sidgwick, *The Organic Chemistry of Nitrogen*, 2nd ed. (Oxford University Press, Oxford, 1937).

[41] H. Sjostrom, L. Hultman, J. E. Sundgren, S. V. Hainsworth, T. F. Page, and G. S. A. M. Theunissen, J. Vac. Sci. Technol. A **14**, 56 (1996).

[42] N. Hellgren, K. Macak, E. Broitman, M. P. Johansson, L. Hultman, and J. E. Sundgren, J. Appl. Phys. **88**, 524 (2000).

[43] H. Sjostrom, S. Stafstrom, M. Boman, and J. E. Sundgren, Phys. Rev. Lett. **75**, 1336 (1995).

[44] K. J. Boyd, D. Marton, S. S. Todorov, A. H. Al-Bayati, J. Kulok, R. A. Zuhr, and J. W. Rabalais, J. Vac. Sci. Technol. A **13**, 2110 (1995).

[45] J. Hu, P. Yang, and C. M. Lieber, Phys. Rev. B **57**, 3185 (1998).

[46] C. A. Davis, D. R. McKenzie, Y. Yin, Kravtchinskaia, G. A. J. Amaratunga, and V. J. Veerasamy, Philos. Mag. B **69**, 1133 (1994).

[47] V. S. Veerasamy, J. Yuan, G. A. J. Amaratunga, W. I. Milne, K. W. R. Gilkes, M. Weiler, and L. M. Brown, Phys. Rev. B **48**, 17 954 (1993).

[48] C. Spaeth, M. Kuhn, U. Kreissig, and F. Richter, Diamond Relat. Mater. **6**, 626 (1997).

[49] B. Kleinsorge, A. C. Ferrari, J. Robertson, and W. I. Milne, J. Appl. Phys. **88**, 1149 (2000).

[50] M. Chhowalla, I. Alexandrou, C. Kiely, G. A. J. Amaratunga, R. Aharonov, and R. Fontana, Thin Solid Films **290−291**, 103 (1996).

[51] X. Shi, H. Fu, J. R. Shi, L. K. Cheath, B. K. Tay, and P. Hui, J. Phys. C **10**, 9293 (1998).

[52] J. K. Walters, M. Kuhn, C. Spaeth, E. Dooryhee, and R. J. Newport, J. Appl. Phys. **83**, 3529 (1998).

[53] X. A. Zhao, C. W. Ong, Y. C. Tsang, Y. W. Wong, P. W. Chan, and C. L. Choy, Appl. Phys. Lett. **66**, 2652 (1995).

[54] K. Ogata, J. F. Diniz, and F. J. Fujimoto, J. Appl. Phys. **76**, 3791 (1994).

[55] N. Takada, K. Arai, S. Nitta, and S. Nonomura, Appl. Surf. Sci. **113**, 274 (1997).

[56] F. R. Weber and H. Oeshner, Thin Solid Films **355/356**, 73 (1999).

[57] J. Bulir, M. Jelinek, V. Vorlicek, J. Zemek, and V. Perina, Thin Solid Films **292**, 318 (1997).

[58] T. Iwasaki, M. Aono, S. Nitta, H. Habuchi, T. Itoh, and S. Nonomura, Diamond Relat. Mater. **8**, 440 (1999).

[59] A. Bousetta, M. Lu, and A. Benasoula, J. Vac. Sci. Technol. A **13**, 1639 (1995).

[60] C. Popov, L. M. Zambov, M. F. Plass, and W. Kulisch, Thin Solid Films **377/378**, 156 (2000).

[61] P. Hammer, N. M. Victoria, and F. Alvarez, J. Vac. Sci. Technol. A **18**, 2277 (2000).

[62] S. E. Rodil, N. A. Morrison, J. Roberston, and W. I. Milne, Phys. Status Solidi A **175**, 25 (1999).

[63] M. Zhang, L. Pan, T. Miyazaki, and Y. Nakayama, Jpn. J. Appl. Phys. **36**, 4897 (1997).

[64] S. Bhattacharyya, C. Cardinaud, and G. Turban, J. Appl. Phys. **83**, 4491 (1998); S. Bhattacharyya, M. Hietschold, and F. Richter, Diamond Relat. Mater. **9**, 544 (2000).

[65] J. Q. Zhang, Y. Setsuhara, S. Miyake, and B. Kyoh, Jpn. J. Appl. Phys. **36**, 6894 (1997).

[66] A. C. Ferrari, A. Libassi, B. K. Tanner, V. Stolojan, J. Yuan, L. M. Brown, S. E. Rodil, B. Kleinsorge, and J. Robertson, Phys. Rev. B **62**, 11 089 (2000).

[67] D. Lin-Bien, N. B. Colthrup, W. G. Fateley, and J. G. Grasselli, *Handbook of Infrared and Raman Characteristic Frequencies of Orgainc Molecules* (Academic, New York, 1991).

[68] I. Chen and R. Zallen, Phys. Rev. **173**, 833 (1968).

[69] R. Alben, D. Weaire, J. E. Smith, and M. H. Brodsky, Phys. Rev. B **11**, 2271 (1975).

[70] J. Knoll and J. Geiger, Phys. Rev. B **29**, 5651 (1984).

[71] M. Bonelli, A. C. Ferrari, A. Fioravanti, A. Li Bassi, A. Miotello, and P. M. Ossi, Eur. Phys. J. B **25**, 269 (2002).

[72] E. Burstein, M. H. Brodsky, and G. Lucovsky, Int. J. Quantum Chem. **1S**, 759 (1967).

[73] G. Lucovsky, R. M. Martin, and E. Burstein, Phys. Rev. B **4**, 1367 (1971).

[74] W. A. Harrison, *Elementary Electronic Structure* (World Scientific, Singapore, 1999).

[75] M. Gussoni, C. Castiglioni, and G. Zerbi, in *Spectroscopy of Advanced Materials*, edited by R. J. Clark and R. E. Hester (Wiley, New York, 1991), p. 251.

[76] J. C. Decius, J. Mol. Spectrosc. **57**, 348 (1975).

[77] U. Dinur, Chem. Phys. Lett. **93**, 253 (1982).

[78] W. L. Peticolas, L. Nafie, P. Stein, and L. Fanconi, J. Chem. Phys. **52**, 1576 (1970).

[79] F. R. Dollish, W. G. Fateley, and F. F. Bentley, *Characteristic Raman Frequencies of Organic Molecules* (Wiley, New York, 1974).

[80] C. Kittel, *Introduction to Solid State Physics* (Wiley, New York, 1967).

[81] G. Zerbi, M. Gussoni, and C. Castiglioni, in *Conjugated Polymers*, edited by J. L. Bredas (Kluwer, Dordrecht, 1991).

[82] E. Ehrenfreund, Z. Vardeny, O. Brafman, and B. Horowitz, Phys. Rev. B **36**, 1535 (1987).

[83] M. Del Zoppo, M. Tommasini, C. Castiglioni, and G. Zerbi, Chem. Phys. Lett. **287**, 100 (1998); C. Castiglioni, M. Tommasini, and M. Del Zoppo, J. Mol. Struct. **521**, 137 (2000).

[84] F. Tuinstra and J. L. Koening, J. Chem. Phys. **53**, 1126 (1970).

[85] C. Castiglioni, F. Negri, M. Rigolio, and G. Zerbi, J. Chem. Phys. **115**, 3769 (2001).

[86] A. Cuesta, P. Dhamelincourt, J. Laureyns, A. Martinez-Alonso, and J. M. D. Tascon, J. Mater. Chem. **8**, 2875 (1998).

[87] P. Lespade, R. Al-Jishi, and M. S. Dresselhaus, Carbon **20**, 427 (1982).

[88] H. Wilhelm, M. Lelaurain, E. McRae, and B. Humbert, J. Appl. Phys. **84**, 6552 (1998).

[89] Y. Wang, D. C. Alsmeyer, and R. L. McCreery, Chem. Mater. **2**, 557 (1990).

[90] R. P. Vidano, D. B. Fishbach, L. J. Willis, and T. M. Loehr, Solid State Commun. **39**, 341 (1981).

[91] *Physical Methods in Heterocycle Chemistry*, edited by A. R. Katkritzki (Academic, New York, 1963); Vols. II, IV.

[92] J. Robertson, Phys. Rev. B **53**, 16 302 (1996).

[93] F. Weich, J. Widany, and T. Frauenheim, Phys. Rev. Lett. **78**, 3326 (1997).

[94] T. Frauenheim, G. Jungnickel, P. Sitch, M. Kaukonen, F. Weich, J. Widany, and D. Porezag, Diamond Relat. Mater. **7**, 348 (1998).

[95] M. Chhowalla, A. C. Ferrari, J. Robertson, and G. A. J. Amaratunga, Appl. Phys. Lett. **76**, 1419 (2000).

[96] W. J. Gammon, D. I. Malyarenko, O. Kraft, G. L. Hoatson, A. C. Reilly, and B. C. Holloway, Phys. Rev. B **66**, 153402 (2002).